DOT-TSC-

CYCLIC INELASTIC DEFORMATION AND FATIGUE RESISTANCE OF A RAIL STEEL: EXPERIMENTAL RESULTS AND MATHEMATICAL MODELS

B. N. Leis
J. H. Laflen

BATTELLE
Columbus Laboratories
505 King Avenue
Columbus, Ohio 43201

June 1977

INTERIM REPORT ON ITEM 11

Document is available to the U.S. public through the
National Technical Information Service,
Springfield, Virginia 22161

Prepared for

U. S. DEPARTMENT OF TRANSPORTATION
FEDERAL RAILROAD ADMINISTRATION
Office of Research and Development
Washington, D. C. 20590

NOTICE

This document is disseminated under the sponsorship of the Department of Transportation in the interest of information exchange. The United States Government assumes no liability for the contents or use thereof.

NOTICE

The United States Government does not endorse products or manufacturers. Trade or manufacturers' names appear herein solely because they are considered essential to the object of this report.

Technical Report Documentation Page

1. Report No. FRA/ORD-81/29	2. Government Accession No.
3. Recipient's Catalog No. PB82 129586	
4. Title and Subtitle: Cyclic Inelastic Deformation and Fatigue Resistance of a Rail Steel: Experimental Results and Mathematical Models	5. Report Date ~~June 1977~~ Oct 1981
	6. Performing Organization Code
7. Author(s): B. N. Leis, J. H. Laflen	8. Performing Organization Report No. G-6265-0006/1
9. Performing Organization Name and Address: Battelle Columbus Laboratories, 505 King Avenue, Columbus, Ohio 43201	10. Work Unit No. (TRAIS) DOT-TSC-80-28
	11. Contract or Grant No. DOT-TSC-1076
12. Sponsoring Agency Name and Address: U. S. Dept. of Transportation, Federal Railroad Administration, Office of Research and Development, Washington, D. C. 20590	13. Type of Report and Period Covered: Interim
	14. Sponsoring Agency Code

15. Supplementary Notes

16. Abstract

Experimental results developed from tests of uniaxial, smooth specimens obtained from the head of an unused section of rail have been reported. Testing encompassed a broad range of conditions - monotonic tension, monotonic compression, and fully reversed constant-amplitude strain cycling. Additionally, a study of "history effects" was made. Included in this study were tests to examine the influence of orientation, mean stress, initial prestrain, and periodic overstrain (both the cyclic deformation response and the fatigue resistance being reported for each condition). Results obtained from the above tests were used to develop mathematical models for rail deformation response and failure. Particular attention has been paid to the influence of stress state on deformation response and fatigue resistance.

17. Key Words: rail steel, monotonic and cyclic deformation, stress, strain, multiaxial, predictive models, history, and fatigue resistance	18. Distribution Statement: Document is available to the public through the National Technical Information Service, Springfield, Virginia 22161

19. Security Classif. (of this report): unclassified	20. Security Classif. (of this page): unclassified	21. No. of Pages	22. Price

Form DOT F 1700.7 (8-72)

* U. S. GOVERNMENT PRINTING OFFICE : 1973 725-504/328

PREFACE

This report presents and discusses experimental results and mathematical models that characterize the cyclic inelastic deformation response and fatigue resistance of a rail steel typical of that used on American railroads. The report was prepared by the Structures and Mechanics Research Department of Battelle's Columbus Laboratories (BCL) for the Transportation Systems Center (TSC) of the Department of Transportation to summarize work performed as a part of Item 11 of Contract No. DOT-TSC-1076, "Rail Material Failure Characteristics". Mr. Roger Steele of TSC was the Technical Monitor.

Experimental results developed from tests of uniaxial, smooth specimens obtained from the head of an unused section of rail have been reported. Testing encompassed a broad range of conditions — monotonic tension, monotonic compression, and fully reversed constant-amplitude strain cycling. Additionally, a study of "history effects" was made. Included in this study were tests to examine the influence of orientation, mean stress, initial prestrain, and periodic overstrain (both the cyclic deformation response and the fatigue resistance being reported for each condition). Results obtained from the above tests were used to develop mathematical models for rail deformation response and failure. Particular attention has been paid to the influence of stress state on deformation response and fatigue resistance.

The experimental work was performed in the Fatigue Labroatory of Battelle's Columbus Laboratories by Mr. Norman Frey, whose work, care, and diligence are gratefully acknowledged. The rail material used in this study was graciously provided by Mr. D. Stone of the Association of American Railways (AAR), Chicago. Mr. Garland Smith of BCL was responsible for the cold rolling reduction of the rail material used in this study.

METRIC CONVERSION FACTORS

Approximate Conversions to Metric Measures

Symbol	When You Know	Multiply by	To Find	Symbol
		LENGTH		
in	inches	*2.5	centimeters	cm
ft	feet	30	centimeters	cm
yd	yards	0.9	meters	m
mi	miles	1.6	kilometers	km
		AREA		
in^2	square inches	6.5	square centimeters	cm^2
ft^2	square feet	0.09	square meters	m^2
yd^2	square yards	0.8	square meters	m^2
mi^2	square miles	2.6	square kilometers	km^2
	acres	0.4	hectares	ha
		MASS (weight)		
oz	ounces	28	grams	g
lb	pounds	0.45	kilograms	kg
	short tons (2000 lb)	0.9	tonnes	t
		VOLUME		
tsp	teaspoons	5	milliliters	ml
Tbsp	tablespoons	15	milliliters	ml
fl oz	fluid ounces	30	milliliters	ml
c	cups	0.24	liters	l
pt	pints	0.47	liters	l
qt	quarts	0.95	liters	l
gal	gallons	3.8	liters	l
ft^3	cubic feet	0.03	cubic meters	m^3
yd^3	cubic yards	0.76	cubic meters	m^3
		TEMPERATURE (exact)		
°F	Fahrenheit temperature	5/9 (after subtracting 32)	Celsius temperature	°C

*1 in = 2.54 (exactly). For other exact conversions and more detailed tables, see NBS Misc. Publ. 286, Units of Weights and Measures, Price $2.25, SD Catalog No. C13.10:286.

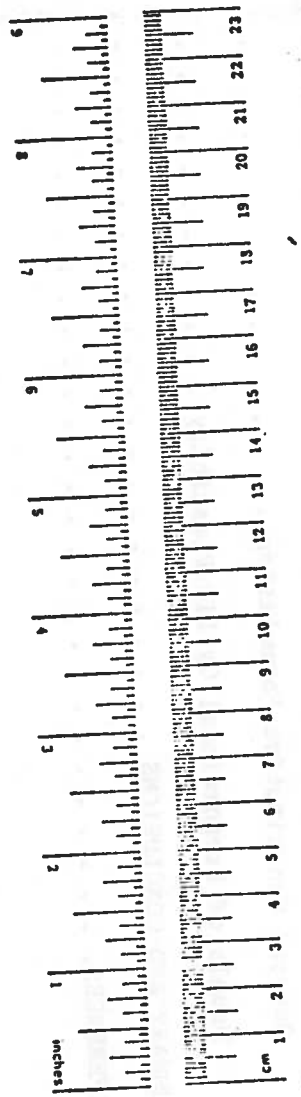

Approximate Conversions from Metric Measures

Symbol	When You Know	Multiply by	To Find	Symbol
		LENGTH		
mm	millimeters	0.04	inches	in
cm	centimeters	0.4	inches	in
m	meters	3.3	feet	ft
m	meters	1.1	yards	yd
km	kilometers	0.6	miles	mi
		AREA		
cm^2	square centimeters	0.16	square inches	in^2
m^2	square meters	1.2	square yards	yd^2
km^2	square kilometers	0.4	square miles	mi^2
ha	hectares (10,000 m^2)	2.5	acres	
		MASS (weight)		
g	grams	0.035	ounces	oz
kg	kilograms	2.2	pounds	lb
t	tonnes (1000 kg)	1.1	short tons	
		VOLUME		
ml	milliliters	0.03	fluid ounces	fl oz
l	liters	2.1	pints	pt
l	liters	1.06	quarts	qt
l	liters	0.26	gallons	gal
m^3	cubic meters	35	cubic feet	ft^3
m^3	cubic meters	1.3	cubic yards	yd^3
		TEMPERATURE (exact)		
°C	Celsius temperature	9/5 (then add 32)	Fahrenheit temperature	°F

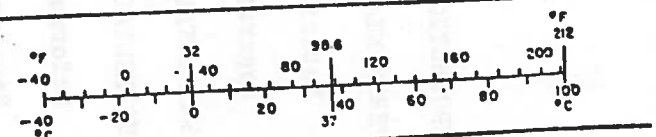

TABLE OF CONTENTS

LIST OF FIGURES

LIST OF FIGURES (Continued)

LIST OF TABLES

INTRODUCTION

In order to determine both the fatigue resistance of new rail and the remaining life of in-service rail, use is made of fatigue damage assessment and accumulation models. When the life to crack initiation of rail is defined as that life after which the progression of a crack can be adequately modeled as a rate process, crack initiation and propagation are both observed to occupy significant fractions of the rails' useful life. In this report, useful life (design) is considered to be that portion of the life until some minimum residual strength level is reached. This level is a function of the material, geometry, and loading and should be chosen with a view for the variable nature of both the loading and the fatigue process. In the context of these two definitions, damage assessment and accumulation models for each of crack initiation and propagation should be integrated into a single "continuing" damage model to make accurate fatigue life assessments for rail.

The purpose of this report is to present the results of a program to develop experimental data for and mathematical models of the cyclic inelastic deformation response and fatigue life of a rail steel useful in performing the initiation and the propagation analyses noted above. These data and mathematical models are also useful in assessing the cycle dependent redistribution of stresses and strains due to rail head plastic flow under service loading. Of particular interest in this context are the inferences of transient material response on the shakedown phenomenon in rail[(1)*].

The results are reported from experiments designed to generate baseline fully reversed strain-controlled fatigue life and cyclic deformation response data for longitudinal and transverse samples cut from an as-rolled, unused section of steel rail. Additionally, both cyclic deformation and fatigue life data developed from studies of mean stress and mechanical history effects are reported. Test conditions designed to simulate certain events encountered in rail service loading were both compression and tension strain-controlled mean stress, initial uniaxial prestrain and periodic overstrain, and rolling induced initial prestrain. When sufficient data are reported or available, mathematical models of the process are developed and discussed herein. The report considers,

---

* References are listed on pages 48 and 49.

in turn, the above noted data in sections entitled Experimental Details, Experimental Results and Discussion, Mathematical Modeling, and Commentary and Conclusions.

EXPERIMENTAL DETAILS

Materials and Specimens

The rail from which specimen blanks were taken for this program was furnished by the Association of American Railways (AAR). Three 6-foot-long pieces cut from a single section of 119-pound-per-yard rail were provided. The chemistry of the rail sample showed its alloy composition in weight percent as 0.82 carbon, 0.87 manganese, 0.035 phosphorous, 0.032 sulfur, 0.21 silicon, and the balance iron, a composition within ASTM Specification A1 for rail steels in the weight range of 91 to 120 except that the carbon content was 0.02 weight percent too high. The microstructure of this nominally eutectoid steel was observed to be pearlite throughout the rail cross section. Figure 1 presents a micrograph typical of this structure. Hardness contours obtained from traverses on a grid in the head and web of the rail were, as expected, symmetric about the longitudinal plane of the rail as shown in Figure 2, part (a). The Rockwell C hardness was in the range from 24 to 25.5 in the central region of the rail head.

With the exception of the tests on material prestrained by rolling, uniaxial cylindrical test specimens with a 0.250-inch diameter by 0.500-inch-long gage section as detailed in Figure 3 were used. These specimens were machined from 13/16-inch square by 5-1/8-inch-long specimen blanks cut symmetrically from the rail head about the longitudinal plane of the rail as shown in Figure 2, part (b). As evident from part (a) of Figure 2, the Rockwell C (R_c) hardness in the reduced section of these longitudinal specimens was about R_c 24 and varied less than one point. Transverse uniaxial test specimens having a reduced section identical to that of the longitudinal test samples were machined from specimen blanks 11/16-inch square by 2-5/8-inch long cut across the rail head as shown in part (c) of Figure 2. This location was chosen to best match the hardness in the reduced section of this transverse specimen with that of the longitudinal specimen.

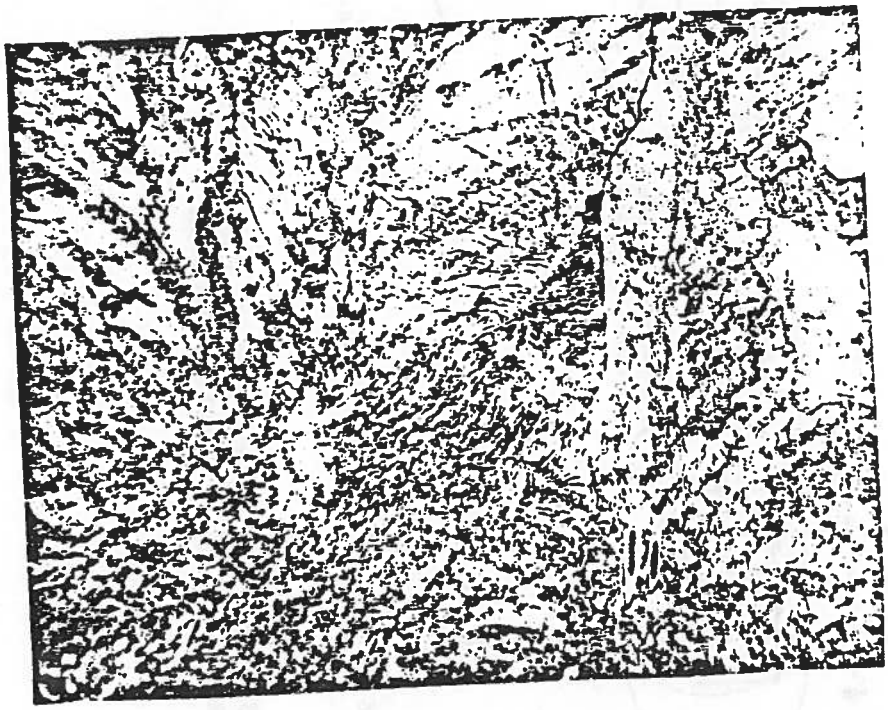

FIGURE 1. PHOTOMICROGRAPH OF THE PEARLITIC STRUCTURE TYPICAL OF THE RAIL HEAD, WEB AND FLANGE MICROSTRUCTURE FOR HOT-ROLLED MATERIAL (FROM THE HEAD); PICRAL ETCHANT

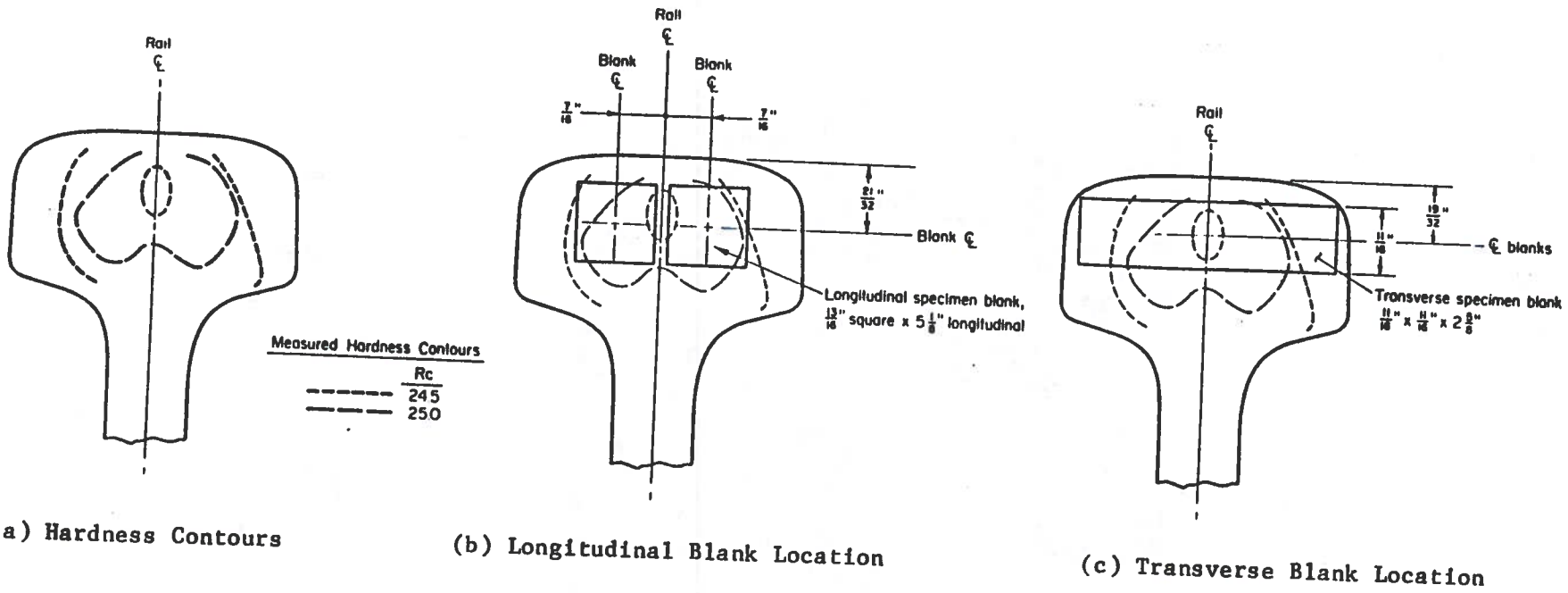

(a) Hardness Contours

(b) Longitudinal Blank Location

(c) Transverse Blank Location

FIGURE 2. HARDNESS CONTOURS AND LOCATIONS OF SPECIMEN BLANKS IN THE RAIL HEAD FOR HOT-ROLLED MATERIAL

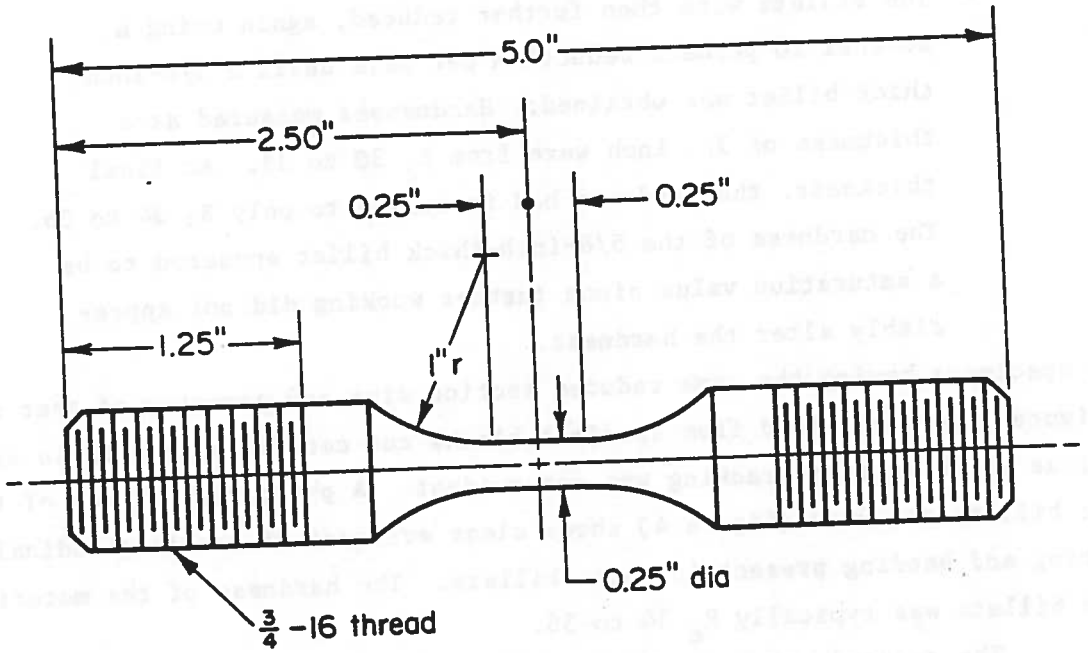

FIGURE 3. LONGITUDINAL UNIAXIAL FATIGUE TEST SPECIMEN

Specimens used in the investigation of material that had been cold worked by rolling were obtained from 5/8-inch square blanks, 4-1/2-inch long cut from the rolled billet. This billet, obtained from the rail head, was reduced according to the following schedule:

- 1-1/4-inch square blanks were reduced using a 20 percent per pass reduction until the blanks were 1-inch square. Rolling was in one direction only. After each pass, the bar was rotated 90 degrees about its longitudinal axis. At this point, any cracked material was cut out.
- The billets were then further reduced, again using a nominal 20 percent reduction per pass until a 5/8-inch-thick billet was obtained. Hardnesses measured at a thickness of 3/4 inch were from R_c 30 to 33. At final thickness, the hardness had increased to only R_c 34 to 36. The hardness of the 5/8-inch-thick billet appeared to be a saturation value since further working did not appreciably alter the hardness.

Test specimens having the same reduced section size and geometry of that shown in Figure 3 were machined from specimen blanks cut centrally from these billets in areas where surface cracking was not evident. A photograph of one of the three billets produced (Figure 4) shows clear evidence of the longitudinal cracking and banding present in these billets. The hardness of the material in these billets was typically R_c 34 to 36.

The reduced section of all test specimens was final machined in 20 passes of not more than 0.001 inch per pass. Samples were subsequently longitudinally polished to yield a finish of about 15 μ rms and then degreased and stored. All specimens were provided with threaded ends. Longitudinal specimen grip ends of both virgin and rolled materials were of sufficient length to preload the specimen grip connection through a locking nut. Transverse samples, however, had insufficient thread length for use of such a preload technique. These samples were preloaded through bearing on a button-head during gripping with care being taken to ensure alignment was maintained.

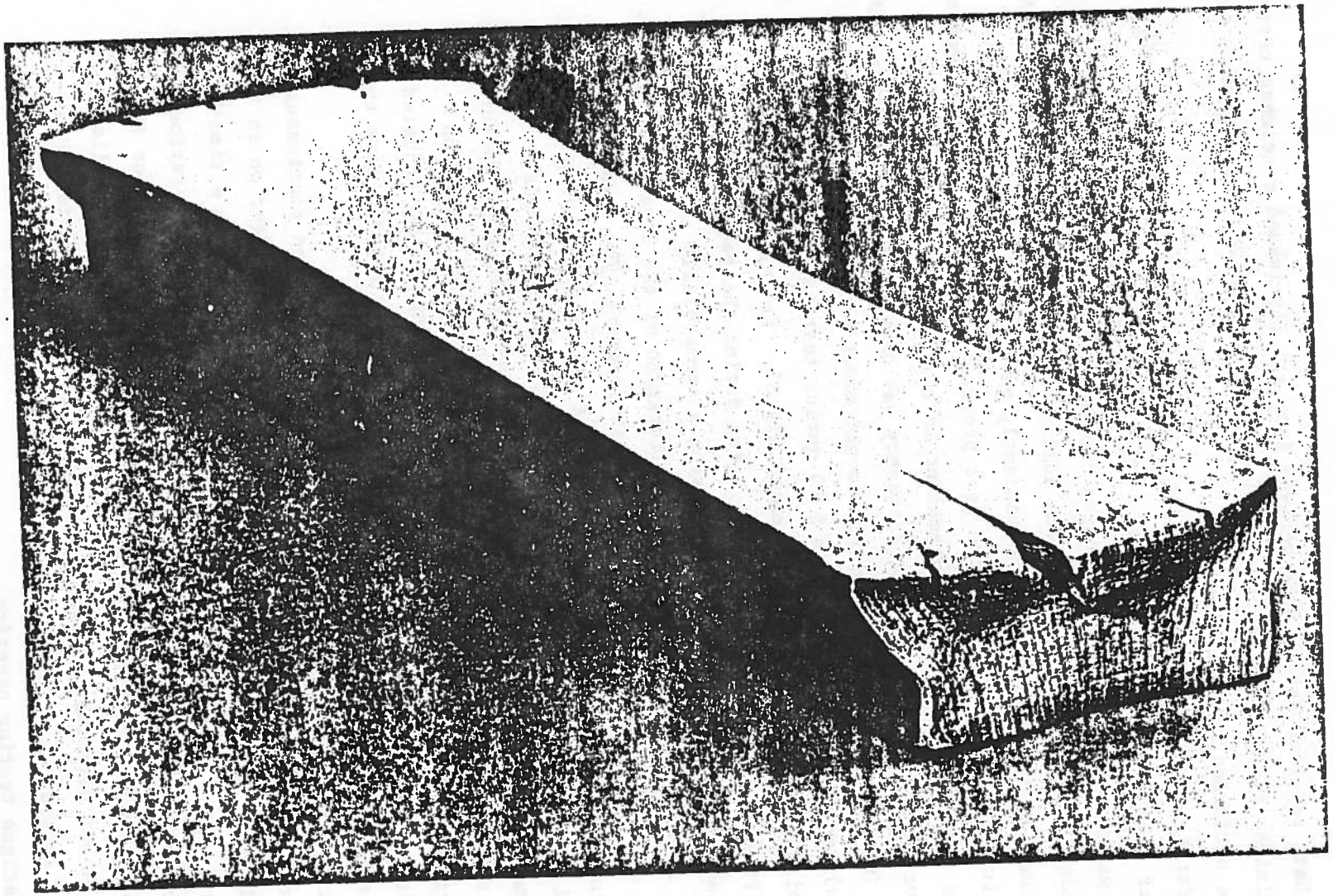

FIGURE 4. PHOTOGRAPH OF A ROLLED BILLET (TYPICAL)

Apparatus and Procedure

Data reported herein were derived from axially loaded specimens tested in three similar closed-loop servocontrolled electrohydraulic test systems. All testing was performed in strain control.

Strain was controlled over a 0.500-inch gage length using a clip-on extensometer calibrated to ASTM Class B_1. Strain was programmed to follow a sinusoidal waveform at frequencies ranging from 0.1 Hz to 30 Hz, depending on the amplitude of the control strain. The ability of the extensometer to operate over this range of frequencies was independently verified as a function of the strain amplitude prior to beginning the test program. To ensure that the temperature of the reduced section remained ambient in tests with either large strain amplitudes or higher frequencies, the frequency was chosen so that the indicated temperature (monitored via a thermocouple looped about and in contact with the test section) remained constant (within 5 F) during testing. Strain was controlled to within 1 percent of the programmed signal. The extensometer calibration was performed and verified several times during the test program.

Load was monitored in all tests using a commercially available load cell mounted in series with the specimen. Calibration of the load cell was performed prior to and verified once during the test program. The load cell was observed accurate and linear within 0.1 percent of the operating range used.

All specimens were gripped in a fixture arrangement similar to that detailed in Reference 2. It is noteworthy that such an arrangement features a liquid-solid Woods metal grip which serves to minimize specimen mounting stresses. Prior to commencing the test program, the alignment was adjusted to minimize bending strains, the adoped standard being bending strains less than 1 percent of the imposed axial strain.

Monotonic and cyclic deformation response was recorded continuously during the first ten cycles and at logarithmic intervals thereafter on an X-Y recorder, while both load and strain were continuously recorded on a time-based high-speed strip chart recorder. Specimens were examined after separation to determine if the failure was representative of the bulk of the metal or if it initiated at some rail processing flaw or inclusion. No detailed metallography of the fractures was performed. All data reported herein were derived from test records in accordance with the ASTM Committee E09.08 draft of a tentative standard for fatigue testing practice.

EXPERIMENTAL PROGRAM

The experimental program consisted of basic materials cyclic inelastic deformation and fatigue life studies. The test matrix followed is presented in Table 1.

EXPERIMENTAL RESULTS AND DISCUSSION

Deformation Response

Consider first the deformation response of the rail steel for each of monotonic and cyclic straining, a study to which 26 specimens have been committed. Data derived from results obtained from monotonic tension, monotonic compression, incremental step and constant amplitude cyclic strain-controlled tests to characterize metal static and cyclic deformation and fatigue life properties after Morrow[3], are reported in Table 2 for both longitudinal and transverse orientations for virgin rail material. Tables 3 and 4 provide a detailed list of other relevant data for each of the specimens tested in this phase of the program. Data used to establish the values of these mechanical properties are shown on coordinates of stress and strain in Figure 5 which presents in part (a) typical deformation response obtained from monotonic tension and compression testing along with that for the first and thirtieth blocks of incremental step cycling for the hot-rolled (HR) material. Part (b) of this figure presents the deformation response of the HR material obtained from stable stress-strain loops developed under constant-amplitude strain cycling; part (c) presents that obtained from specimens oriented transverse to the longitudinal axis of the rail, also for HR material. Finally, part (d) presents the monotonic and cyclic deformation response for cold rolled (CR) samples of the HR material. For this report, a stress-strain loop is said to be stable if the cyclic rate of change in stress is less than 10^{-6} ksi/cycle. Results shown in Figure 5(b) characterize the metal's deformation response in terms of isocycle lines at cycle numbers of 1 (static tension), 10, 10^2, 10^3, and 10^6. Note that at higher strain amplitudes ($\Delta e^t/2 > 0.15$ percent), the deformation response for the longitudinal samples at cycle numbers greater than 10^4 is virtually coincidental.

TABLE 1. EXPERIMENTAL PROGRAM[a]

Test Type	Material[b] Condition	Specimens[c] Utilized	Remarks
		Longitudinal	
Monotonic Tension	HR	4,5,19,44	--
Montonic Compression	HR	3,23	--
Incremental Step	HR	10,29,42	--
	CR	52	Step test run only 2 blocks; samples then used for life studies
Block	CR	51	--
Fully Reversed	HR	1,8,9,13,14,17, 20,21,22,50	--
	CR	52	--
Tension Mean Stress	HR	2,25,27,38,40,48	--
Compression Mean Stress	HR	6,7,15,24,35,39, 49	--
	CR	53	--
Prior History Effects	HR	12,28,32	Compression precycling.
Subsequent History Effects (Sequence)	HR	36,43	Periodic overstrain – tension mean stress
		45	Periodic overstrain – zero mean stress
		16	Periodic overstrain – compression mean stress
		Transverse	
Fully Reversed	HR	T1,T2,T3,T4	--

(a) All tests run in strain control.
(b) HR – as received hot rolled; CR – cold rolled to R_c 34 to 36.
(c) Specimens 11, 18, 26, 30, 31, 33, 34, 41, 46, and 47 for HR material were spares; Specimen 37 was used as a setup dummy sample.

TABLE 2. AVERAGE DEFORMATION AND FATIGUE PROPERTIES OF THE RAIL STEEL (LONGITUDINAL ORIENTATION EXCEPT AS NOTED)

Monotonic Properties[a]	Cyclic Properties[d]
Mod. of Elast., E, 28.85 (28.25)[b] x 10^3 ksi	Proportional Stress, 42.10 ksi
Yield Strength, 0.2%, 70.08 (71.7) ksi	Strain Hrd. Exp., n', 0.239[c,e]
Ultimate Strength, 134.6 ksi	Strength Coeff., K', 88.63[c,e] ksi
Red. in Area, 14.70%	Fatigue Strength Coeff., S'_f, 187.5[c] ksi
True Frac. Strength, 151.6 ksi	Fatigue Ductility Coeff., e'_f, 0.22[f]
True Frac. Ductility, 0.159	Fatigue Strength Exp., b, -0.096[f]
Strain Hrd. Exp., 0.163[c]	Fatigue Ductility Exp., c, -0.493[f]
	Transition Life, $2N_t$, 7125[g] reversals

(a) Average of four tests.

(b) Values in parenthesis are for transverse specimens; average of two tests.

(c) Also characteristic of the transverse orientation.

(d) Data derived from a total of ten tests.

(e) Parameters in the stress-strain equation $S = K'e_p^{n'}$; where s and e_p are stress and plastic strain amplitudes, respectively.

(f) Parameters in the strain life equation $\frac{\Delta e^t}{2} = \frac{S'_f}{E}(2N_f)^b + e'_f(2N_f)^c$; where $\Delta e^t/2$ is the total strain amplitude corresponding to a life to failure of N_f cycles or $2N_f$ reversals.

(g) The life at which the quantities $\frac{S'_f}{E}(2N_f)^b$ and $e'_f(2N_f)^c$ are equal.

TABLE 3. RESULTS FROM MONOTONIC LOADING TESTS

Properties	Specimen Number 4	5	19	44	Average
Monotonic Tension					
Modulus of Elasticity, x 10^3 ksi	29.8	28.5	28.0	29.1	28.85
Yield Strength (0.2% Offset), ksi	70.2	69.9	69.3	70.9	70.1
Ultimate Strength, ksi	--	134.2	134.1	135.4	134.6
True Fracture Strength, ksi	--	151.6	151.6	151.4	151.5
True Fracture Strain, in./in.	0.147	0.161	0.172	0.156	0.159
Reduction in Area, 0/01 %	13.7	14.9	15.8	14.4	14.7

Monotonic Compression

Properties	Specimen No. 3	23	Average
Modulus of Elasticity, x 10^3 ksi	28.0	28.5	28.25
Yield Strength (0.2% Offset), ksi	72.5	71.2	71.8

TABLE 4. RESULTS FROM FULLY REVERSED STRAIN CONTROLLED, CYCLIC LOADING TESTS

Specimen Number	Material Condition	Strain Range, percent		Stress[a] Range, ksi	Life, cycles	
		Total	Plastic[a]		Initiation[b]	Separation
			Longitudinal Orientation			
50	HR	3.03	2.28	207.16	289	300
9	HR	2.04	1.38	182.6	850	976
8	HR	1.04	0.51	141.6	4,800	5,080
22	HR	0.91	0.42	131.1	7,600	7,760
17	HR	0.75	0.28	123.0	14,170	15,178
13	HR	0.526	0.136	109.0	29,690	30,111
21	HR	0.504	0.126	106.2	40,420	43,490
1	HR	0.47	0.10	102.9	53,800	55,600
20	HR	0.37	0.034	93.8	627,400	641,100
14	HR	0.28	--	--	R/O	$>5.6 \times 10^6$
52[c]	CR	0.73	0.11	181.8	11,650	12,547
			Transverse Orientation			
T-1		1.01	0.54	140.0	1,116	1,232
T-2		1.04	0.50	141.1	1,438	1,713
T-3		0.72	0.26	117.37	4,000	4,946
T-4		0.36	0.03	91.0	--	53,836

(a) Values listed are stable values or values computed at one half of the life to failure.
(b) Crack initiation obtained from a back extrapolation of the asymmetric decrease in tensile load from the load-time record.
(c) Test preceeded by two blocks of an incremental step test to 2 percent range.

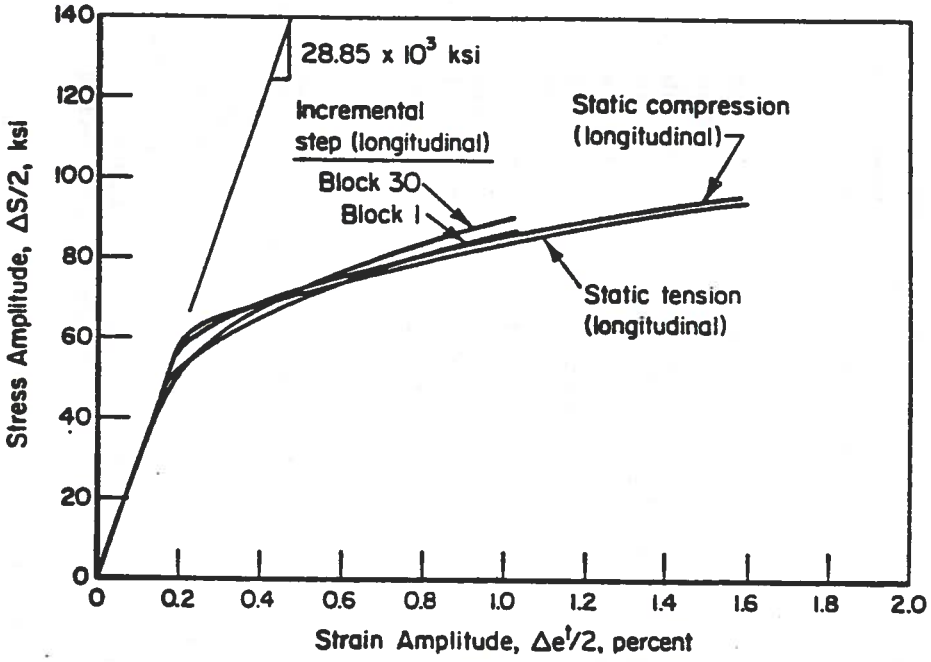

(a) Monotonic Tension, Monotonic Compression and Incremental Step Test for Hot-Rolled Material Stress-Strain Curves

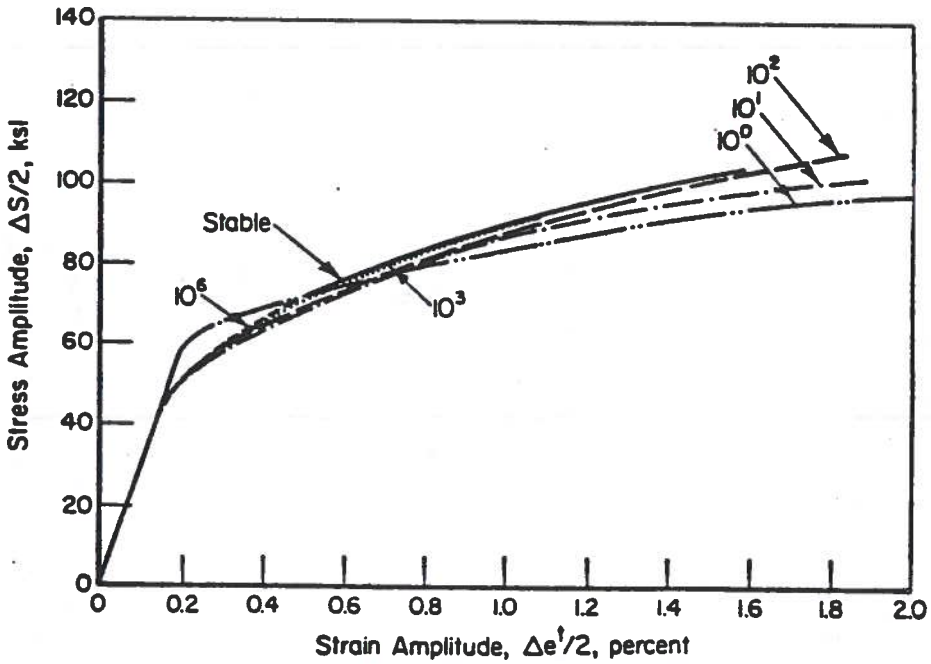

(b) Transient Cyclic Stress-Strain Curves for Hot-Rolled Material

FIGURE 5. MATERIAL MONOTONIC AND CYCLIC STRESS-STRAIN RESPONSE

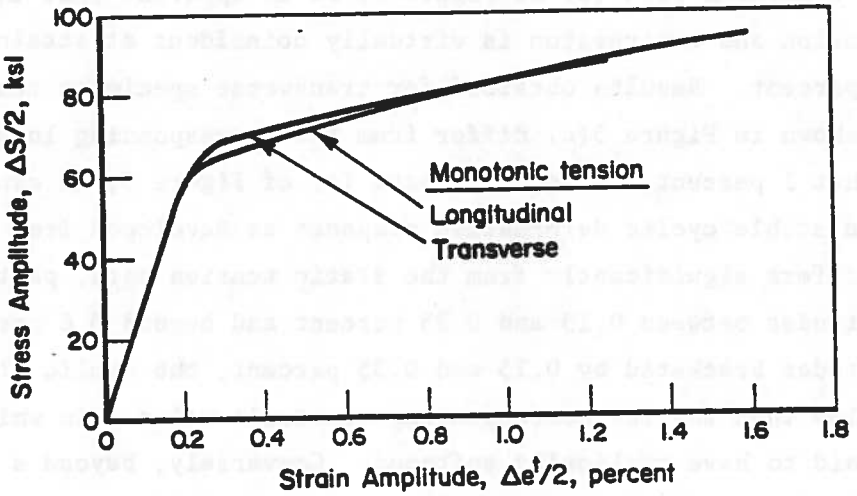

(c) Comparison of Monotonic Tension Results for Longitudinal and Transverse Orientations for Hot-Rolled Material

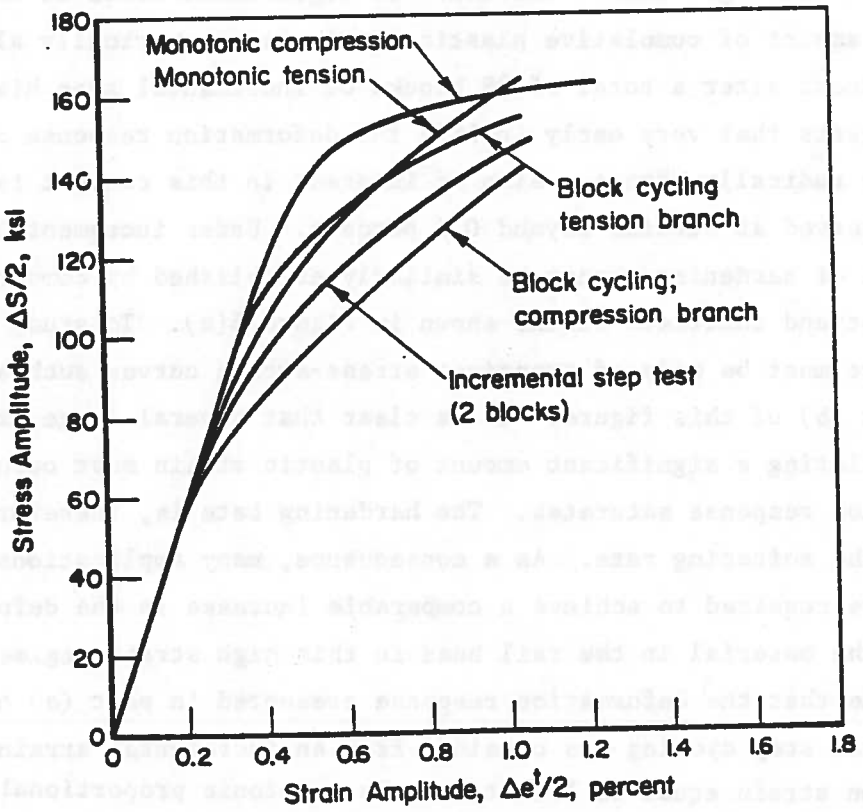

(d) Monotonic and Cyclic Stress-Strain Response for Cold-Rolled Material

FIGURE 5. (Continued)

Upon examining part (a) of Figure 5, it is apparent that the monotonic response in tension and compression is virtually coincident at strain levels less that 1.5 percent. Results obtained for transverse specimens tested in monotonic tension shown in Figure 5(c) differ from the corresponding longitudinal data by less that 1 percent. Also, from part (a) of Figure 5, it can be observed that the stable cyclic deformation response as developed from incremental step testing differs significantly from the static tension data, particularly at strain amplitudes between 0.15 and 0.35 percent and beyond 0.6 percent. In the range of amplitudes bracketed by 0.15 and 0.35 percent, the cyclic stress response lies below that for the corresponding monotonic value — in which case the metal is said to have cyclically softened. Conversely, beyond a strain of 0.6 percent, the cyclic stress response lies above the monotonic curve indicating the metal has cyclically hardened.

Note that a major fraction of the cyclic softening occurred in the first block of loading. This observation is significant since it indicates only a small amount of cumulative plastic strain causes virtually all of the softening evident after a total of 38 blocks of incremental step history. This behavior suggests that very early in life the deformation response of the metal in a rail may radically change. Also of interest in this context is the cyclic hardening observed at strains beyond 0.6 percent. Under incremental step loading, the rate of hardening cannot be similarly established by comparing data from the first and thirtieth blocks shown in Figure 5(a). To study the rate of hardening, use must be made of transient stress-strain curves such as those shown in part (b) of this figure. It is clear that several large amplitude cycles accumulating a significant amount of plastic strain must occur before the deformation response saturates. The hardening rate is, therefore, less as compared to the softening rate. As a consequence, many applications of higher loads would be required to achieve a comparable increase in the deformation response of the maserial in the rail head in this high strain regime.

Note that the deformation response presented in part (a) of Figure 5 for incremental step cycling was obtained from an incremental straining about a mean tension strain equal to 1.10 times the monotonic proportional strain. This condition was imposed so as to relax any residual stress induced during the rail's manufacture. Stress response developed during this test virtually matched that obtained during a similar test without the mean strain. Such a result indicates that the manufacture of rail does not induce significant residual stresses in the region from which the longitudinal samples were obtained.

The monotonic and cyclic deformation response obtained from samples cut from blanks of the CR rail steel (R_c 34 to 36) is substantially different than that discussed previously in the context of the as-received HR material. This is clearly evident by comparing the respective behaviors of the HR and CR materials shown in Figures 5(a) and 5(d). With reference to the monotonic results, note that the response for the CR material shows it to be almost two times as "strong" as the HR material in terms of yield strength. Note also that the results indicate the material is stronger in compression than in tension, at least at strains less than about 0.8 percent. At strains greater than 0.75 percent, the results indicate that the tension and compression curves will cross. Thus, beyond 0.75 percent, the CR material may be stronger in tension than compression. In any event, the difference between the response in tension and compression in the longitudinal samples is small (less than 3 percent in the 0.2 percent off-set yield stress). Such is, of course, expected in view of the cold rolling prior history.

The cyclic deformation response for the CR material also shows it to be somewhat stronger than the HR material as evident in a comparison of the results plotted in Figures 5(a) and 5(d). Note that this behavior does not necessarily relate to the corresponding behavior observed in the monotonic loading data. Indeed usually, as reported by Dugdale[4] and later by Morrow[3], "the (initial) strain history leaves no lasting effect" on the ensuing steady state deformation response. Consequently, transient deformation response can be expected to return the deformation response of the CR material to a condition approximating that observed for the HR state. The above noted tendancy is observed in the curves denoted "cyclic" in Figure 5(d). Note that these cyclic curves represent data obtained from (1) a block cycling test and (2) an incremental step test[3]. (For purposes of the block cycle test, the loading program commenced at a strain level just beyond yield and continued at that strain range for a number of cycles until the transient change per cycle was on the order 5×10^{-2} ksi/cycle. Then, and thereafter, each time the rate of transient response approached that rate, the strain-range was increased by about 10 percent of the current range.)

Both sets of cyclic stress-strain curves exhibit a small tensile mean stress (about 12 ksi in 240 ksi range) under fully reversed strain cycling.

This is evident in the apparent differences in the relative strengths of the material properties in tension and compression observed in both the monotonic and cyclic data. Such a small mean stress, while not expected as a result of the prestrain in rolling, can be attributed to the nonhomogeneous nature of the deformation evident in portions of the billets from which the CR specimens were cut (see Figure 4). If this is the cause, the attendant mean stress could be either tensile or compressive and can be expected to "washout" under reversed inelastic strain cycling as evident in the converging curves for tension and compression data obtained at larger strain levels in the block cycle test. In this context, it is important to point out that neither set of cyclic curves characterize the "stable" cyclic response since the block cycling changed strain ranges at a transient rate of 5×10^{-5} ksi/cycle and the incremental step cycling terminated after only 2 blocks. As such, further (possibly extensive) softening can occur along with continued mean stress relaxation. The former results in a continuing decrease in deformation resistance from the monotonic CR stress-strain curve toward the stable cyclic response of the HR material. (This same trend is being observed in current work on cold worked rail steels being performed at the AAR[5].) The latter results in a stable cyclic stress-strain response which is symmetric in tension and compression.

Mathematical models of the deformation response shown in Figure 5 and discussed above have been developed as detailed later in the Mathematical Models section.

The dependence of the stress response on the number of strain cycles for the HR material shown in Figure 5(b) is more easily studied when these same data are replotted on coordinates of stress amplitude and cycles as in Figure 6(a). A significant feature of the rail steel's cyclic deformation response evident in this figure is that even at endurance strain levels the material softens continuously with cycles as shown by the data for the 0.14 percent amplitude test. Because the driving force for this softening is the presence of inelastic strain and because with softening the magnitude of this inelastic component increases, this softening continues with further cycling. As a consequence of this softening at strains below the endurance strain, the use of elasticity analyses in fatigue life prediction models for rails may lead to significantly inaccurate estimates of the stress-strain fields about inclusions, rail bolt holes, and the like. Stress response obtained as a function of

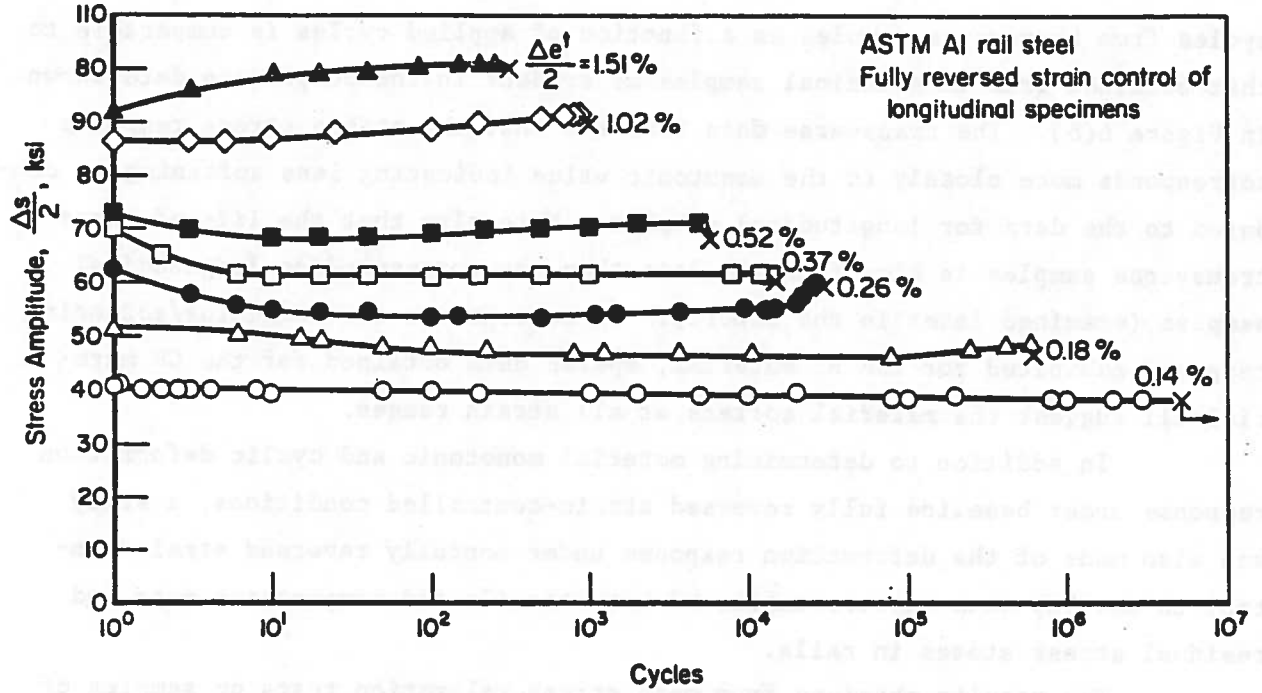

(a) Longitudinal Stress Response

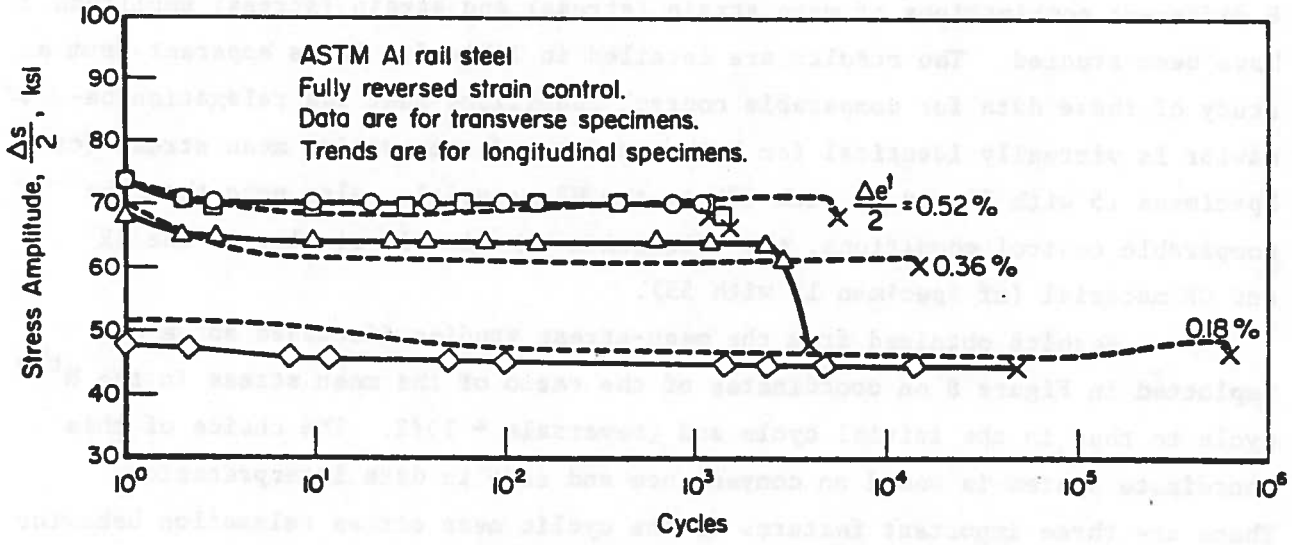

(b) Comparison of Stress Response for Longitudinal and Transverse Orientations

FIGURE 6. DEPENDENCE OF THE STRESS RESPONSE ON THE NUMBER OF STRAIN CYCLES FOR HOT-ROLLED MATERIAL

cycles from transverse samples as a function of applied cycles is comparable to that obtained from longitudinal samples as evident in the comparison data shown in Figure 6(b). The transverse data indicate that the stable stress response corresponds more closely to the monotonic value indicating less softening as compared to the data for longitudinal samples. Note also that the life of these transverse samples is significantly less than the corresponding longitudinal samples (examined later in the report). In contrast to the hardening/softening response exhibited for the HR material, sparse data obtained for the CR material all suggest the material softens at all strain ranges.

In addition to determining material monotonic and cyclic deformation response under baseline fully reversed strain-controlled conditions, a study was also made of the deformation response under nonfully reversed strain control to develop data representative of both tensile and compressive mean and residual stress states in rails.

The results obtained from mean stress relaxation tests on samples of HR and CR materials are presented in parts (a) to (f) of Figure 7. A total of 14 samples were used in this study which examined the influence of both peak strain and strain amplitude on the relaxation behavior. All together, 8 different combinations of mean strain (stress) and strain (stress) amplitude have been studied. The results are detailed in Table 5. It is apparent from a study of these data for comparable control conditions that the relaxation behavior is virtually identical for both tension and compression mean stress (cf Specimens 15 with 38 and 39 with 48) in the HR material. Also note that for comparable control conditions, the relaxation behavior is similar in the HR and CR material (cf Specimen 15 with 53).

Results obtained from the mean-stress studies discussed above are replotted in Figure 8 on coordinates of the ratio of the mean stress in the N^{th} cycle to that in the initial cycle and (reversals + 1)/2. The choice of this coordinate system is based on convenience and ease in data interpretation. There are three important features of the cyclic mean stress relaxation behavior of this rail steel evident in this form of data presentation. First, the rate of relaxation manifest in the negative slope (more negative slopes indicating higher rates) is essentially identical for both tensile and compressive mean stress under comparable control conditions for material in the HR condition.

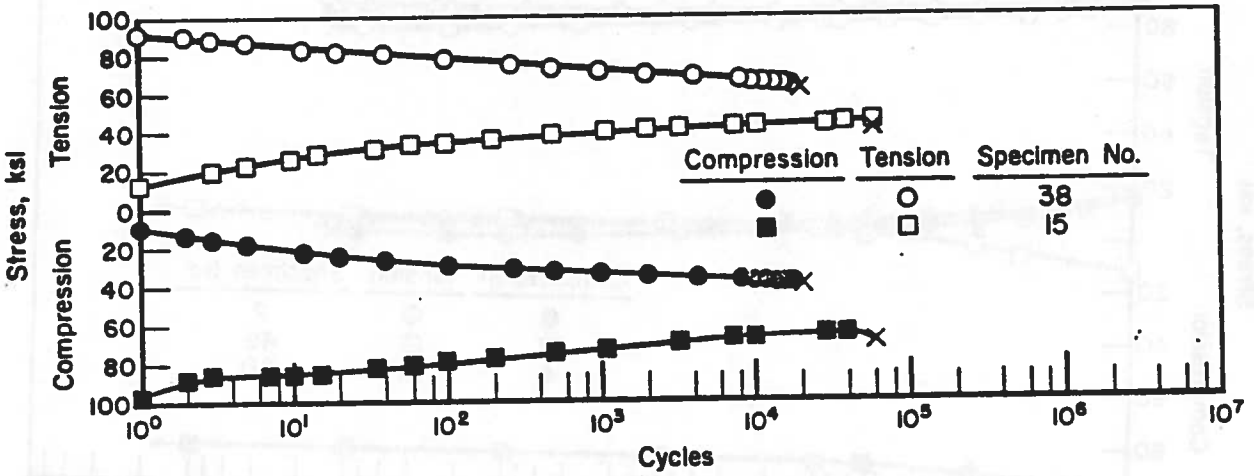

(a) Relaxation Behavior for Hot-Rolled Material;
Strain Range 0.558 Percent

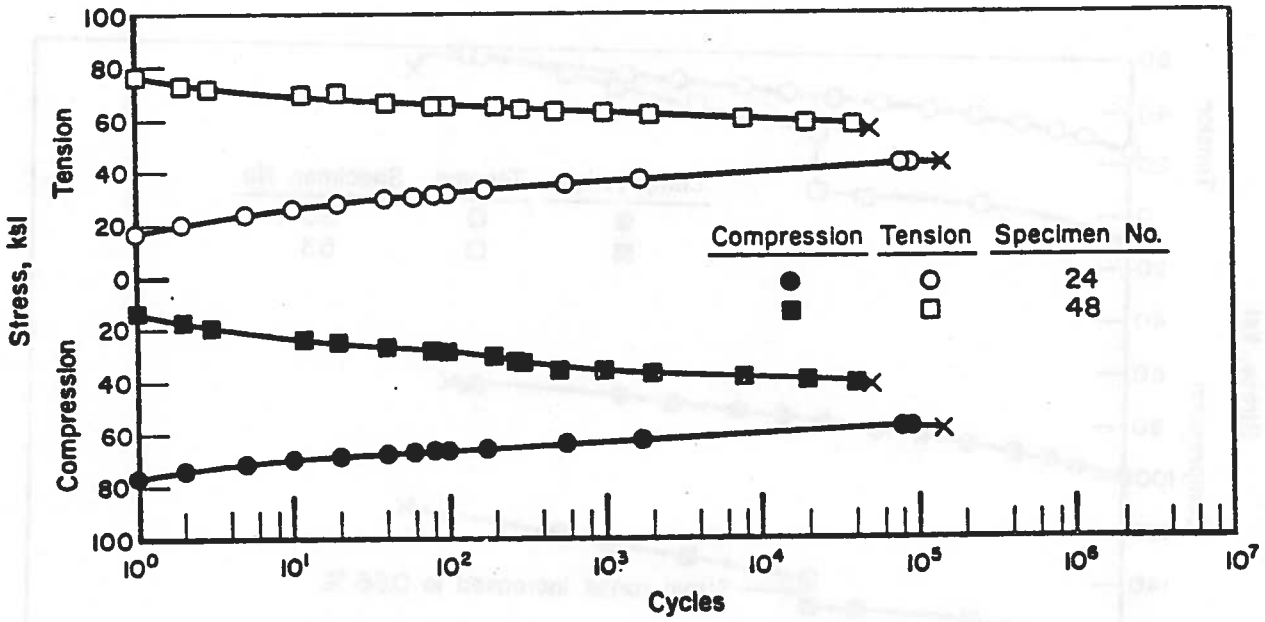

(b) Relaxation Behavior for Hot-Rolled Material;
Strain Ranges of 0.41 and 0.44 Percent

FIGURE 7. MEAN STRESS RELAXATION IN A RAIL STEEL
(INCLUDES BOTH HR AND CR MATERIALS)

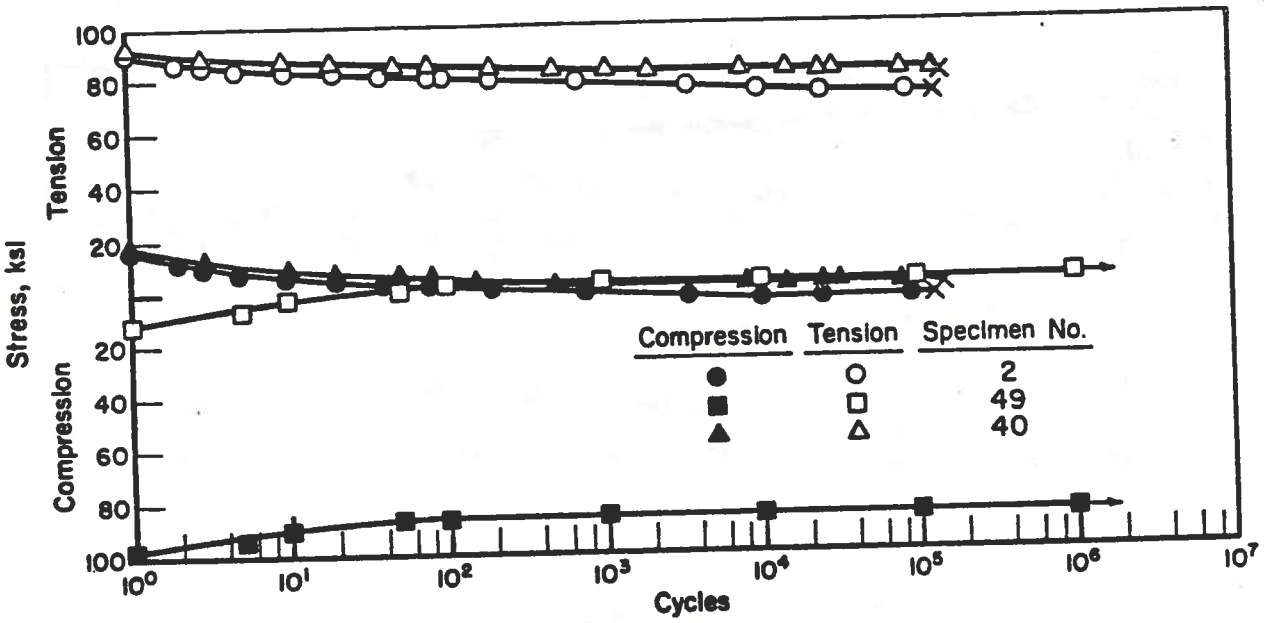

(c) Relaxation Behavior for Hot-Rolled Material; Strain Range of 0.32 Percent

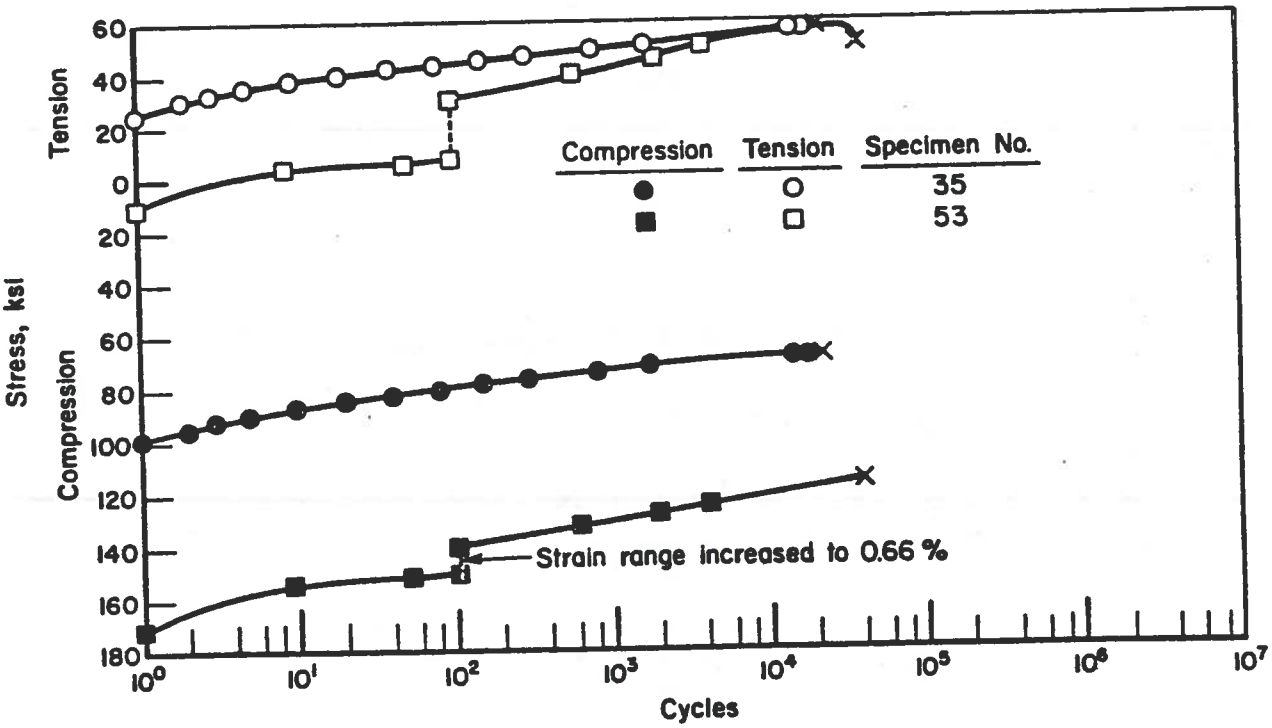

(d) Comparison of Relaxation Behavior for HR and CR Material; Strain Ranges of 0.66 and 0.67 Percent

FIGURE 7. (Continued)

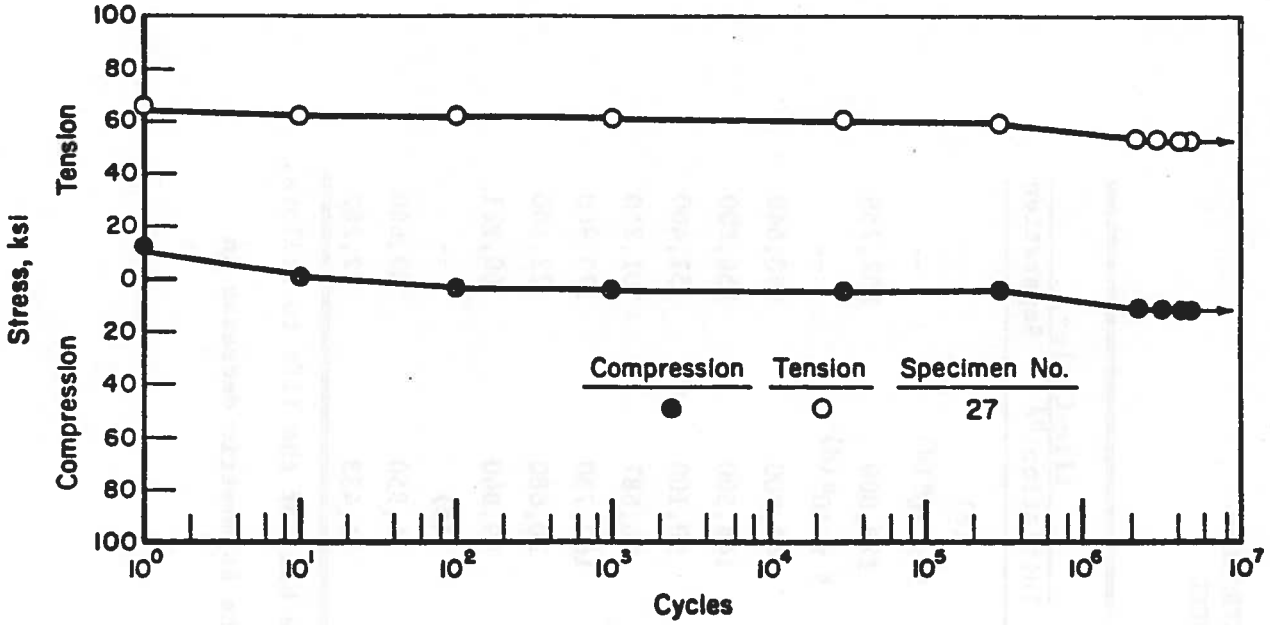

(e) Relaxation Behavior for Hot-Rolled Material;
Strain Range of 0.22 Percent

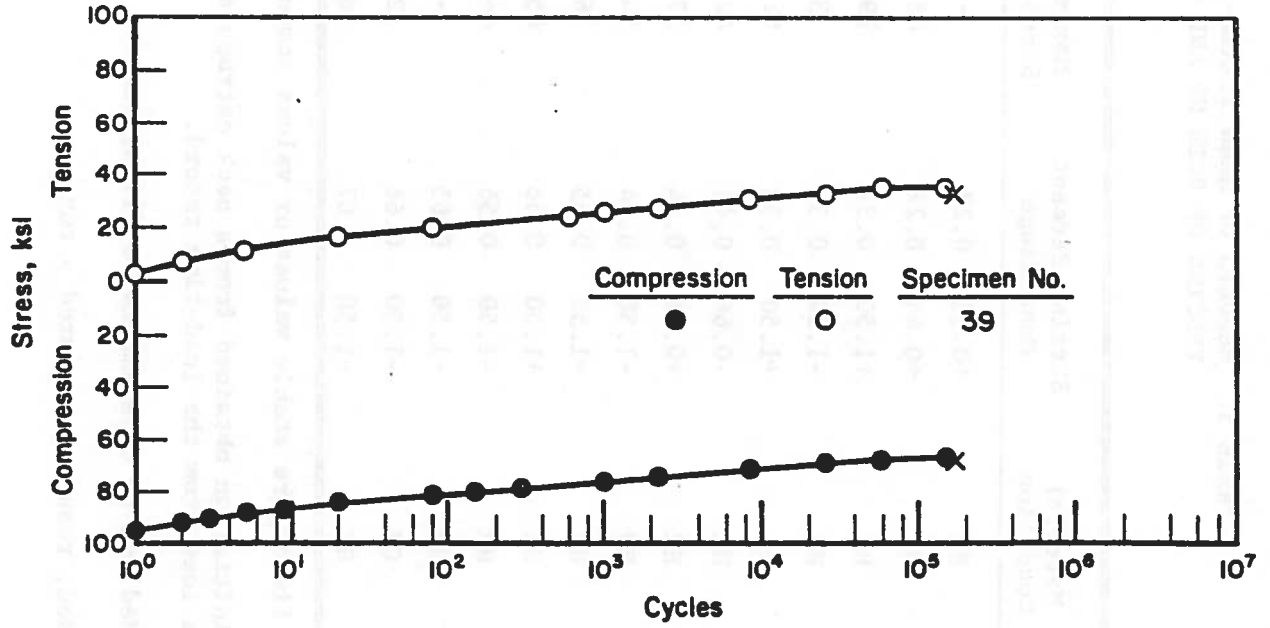

(f) Relaxation Behavior for Hot-Rolled Material;
Strain Range of 0.45 Percent

FIGURE 7. (Continued)

TABLE 5. RESULTS OF MEAN STRAIN-STRAIN CONTROLLED TESTING OF BOTH HR AND CR RAIL STEEL

Specimen Number	Material Condition	Strain, Percent Mean	Strain, Percent Range	Maximum[a] Stress, ksi	Life Cycles, Initiation[b]	Life Cycles, Separation
25	HR	+0.33	0.22	--	(c)	--
27	HR	+0.44	0.22	48.4	5×10^8 (d)	--
40	HR	+1.50	0.32	79.3	129,000	132,759
49	HR	-1.50	0.32	3.7	5×10^8 (d)	--
2	HR	+1.50	0.33	82.0	142,000	150,640
24	HR	-0.66	0.41	42.1	146,500	156,800
48	HR	+0.66	0.44	57.4	50,100	51,400
7	HR	-1.50	0.44	34.0	96,687	101,250
39	HR	-1.50	0.45	36.0	167,730	179,960
38	HR	+1.50	0.56	65.5	20,680	22,600
15	HR	-1.50	0.56	44.2	59,840	60,921
6	HR	-1.50	0.65	--	(c)	--
53	CR	-1.50	0.66	52.4	34,950	39,660
35	HR	-1.50	0.67	56.0	21,433	22,282

(a) Values listed are stable values or values computed at one half of the life to failure.

(b) Crack initiation obtained from a back extrapolation of the asymmetric decrease in tensile load from the load-time record.

(c) Suspended due to experimental difficulties.

(d) Suspended, result considered a run-out.

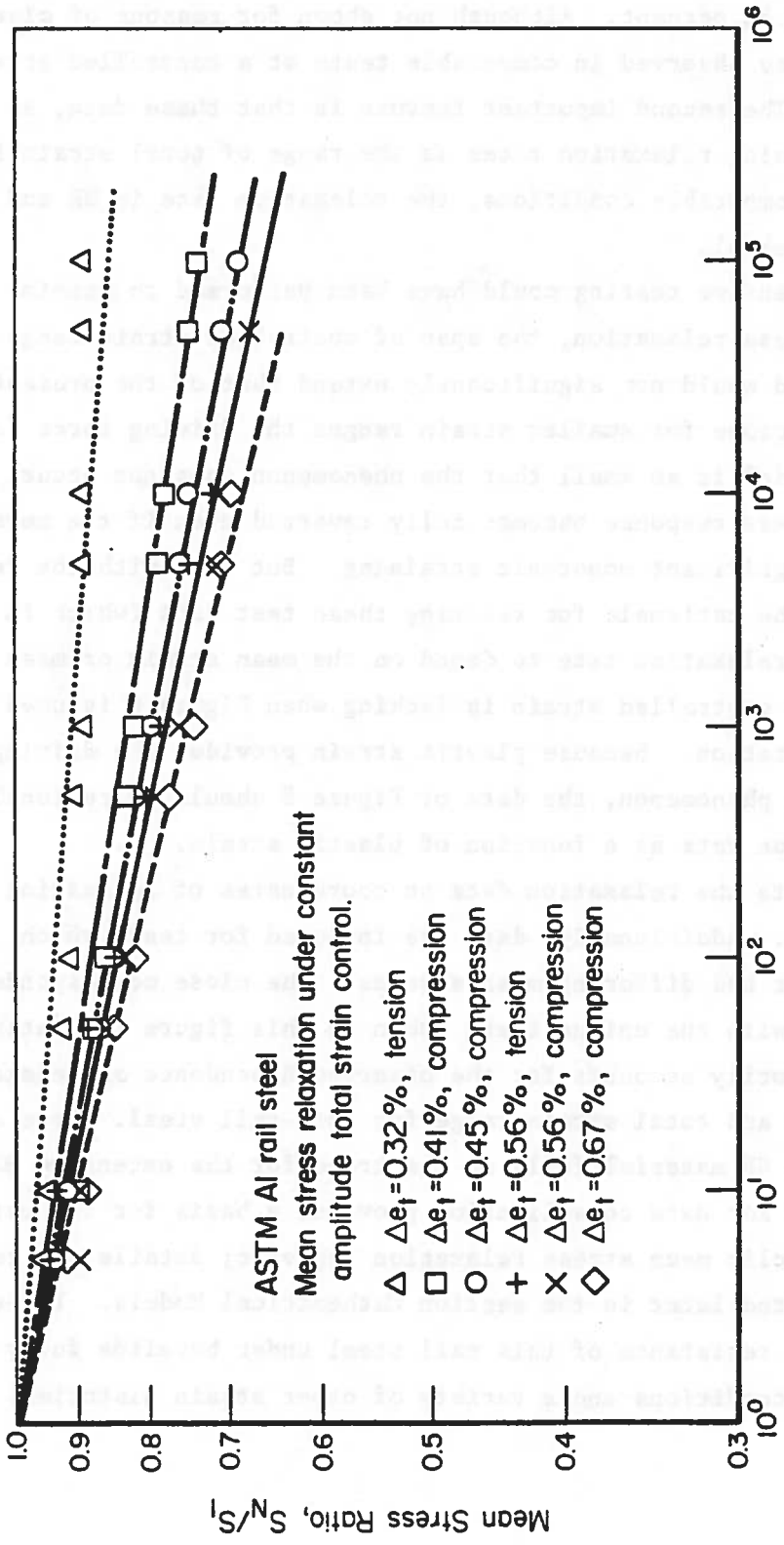

FIGURE 8. DEPENDENCE OF THE MEAN STRESS RATIO ON THE NUMBER OF STRAIN CYCLES

In this figure, such a response is apparent in the data presented for a controlled cyclic strain range of 0.56 percent. Although not shown for reasons of clarity, this same behavior is also observed in comparable tests at a controlled strain range of 0.45 percent. The second important feature is that these data, as would be expected, show increasing relaxation rates as the range of total strain increases. Third, under comparable conditions, the relaxation rate in HR and CR material is essentially equal.

While more extensive testing could have been performed to examine cycle dependent mean stress relaxation, the span of controlled strain ranges which can be investigated would not significantly extend that of the present investigation. This is because for smaller strain ranges the driving force for relaxation (plastic strain) is so small that the phenomenon does not occur, while at larger ranges the stress response becomes fully reversed even if the metal is initially hardened by significant monotonic straining. But even with the results of additional testing, the rationale for relating these test data (which in this investigation shows the relaxation rate to depnd on the mean strain or mean stress) and the range of controlled strain is lacking when Figure 8 is used as a format for data interpretation. Because plastic strain provides the driving force for this transient phenomenon, the data of Figure 8 should be rationalized by plotting the relaxation rate as a function of plastic strain.

Figure 9 replots the relaxation data on coordinates of relaxation rate and plastic strain range. Additionally, data are included for tests which shared a common range but had differing mean strains. The close correspondence of all relaxation rates with the unique trend shown in this figure indicates plastic strain satisfactorily accounts for the observed dependence of relaxation rate on mean strain and total strain range for this rail steel. Note also that the behavior of the CR material falls on the trend for the extensive HR data set. Such a format for data consolidation provides a basis for the mathematical model of this cyclic mean stress relaxation behavior; details and results of which are reported later in the section Mathematical Models. Let us next examine the fatigue resistance of this rail steel under baseline fully reversed strain control conditions and a variety of other strain histories.

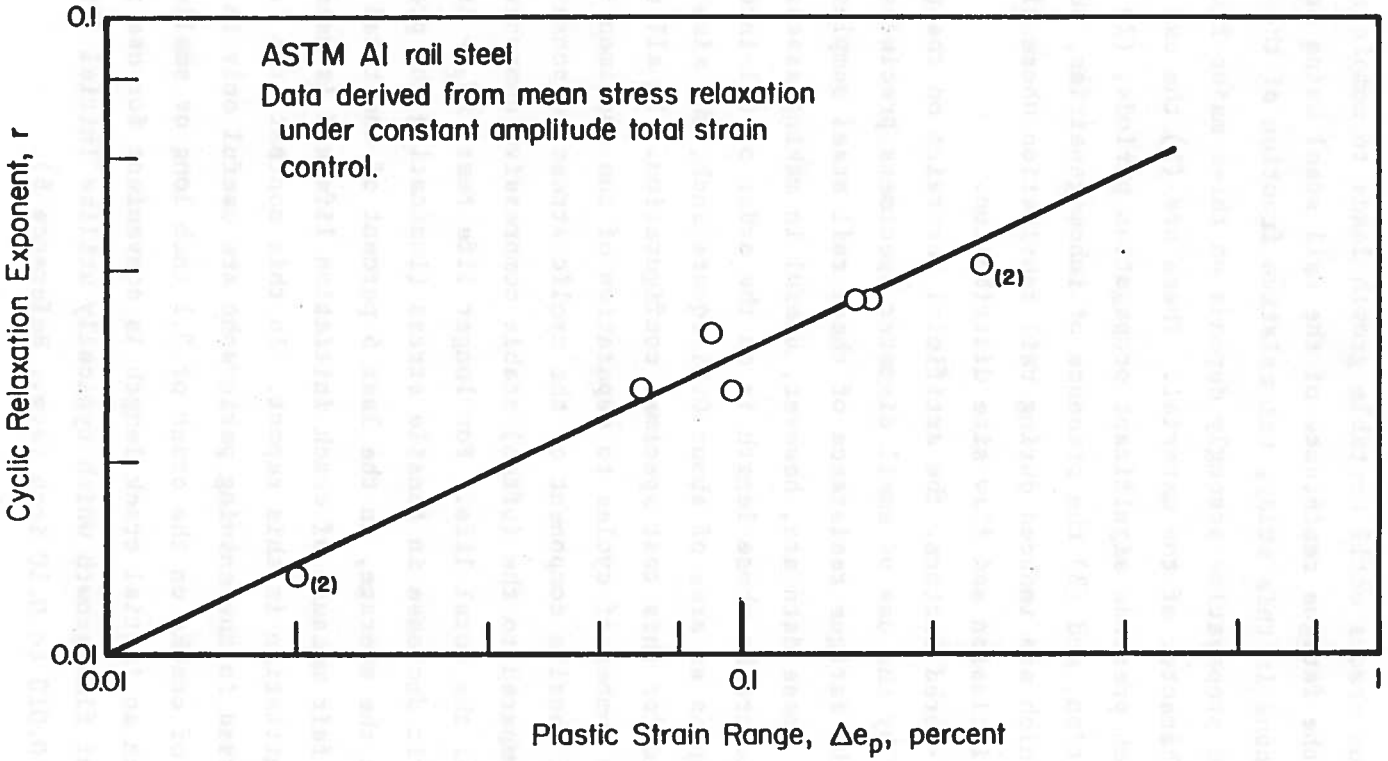

FIGURE 9. CYCLIC RELAXATION EXPONENT AS A FUNCTION OF THE PLASTIC STRAIN RANGE

Fatigue Resistance

As noted in the introduction, the fatigue life of a metal, be it in use in a structure or in a test in the laboratory, is spent first initiating then propagating fatigue cracks until unstable growth leads to complete separation. When examining the fatigue resistance of the rail steel using uniaxial test specimens as was done in this study, the relative fraction of the total life spent in initiation and propagation strongly depends on three major factors in addition to the bulk character of the material. These are (1) the use of small diameter specimens which preclude significant propagation periods, (2) the definition of crack initiation, and (3) the presence of inhomogeneities, such as inclusions and flaws which are induced during rail fabrication whose size represent the tails of the inclusion and flaw size distribution.

Of the above-noted factors, the artificial restraint on the propagation period introduced by the use of small diameter specimens precludes the direct comparison of the fatigue resistance of these rail steel samples with that for actual rail. These data are, however, useful in making assessments of the life to initiate cracks whose length is on the order of 0.1-inch long and whose surface occupies an area of about 0.01 square inch, the size and area typically observed for this test specimen configuration. In all cases for data reported, the number of cycles to separation of the specimen differed from that at which the tensile component of the cyclic stress response first began decreasing as compared to the (often) stable compressive component by less than 13 percent of the total life. For longer life tests ($N_f > 10,000$ cycles), this asymmetric decrease in tensile stress (indicating the presence of a crack) occurs, on the average, in the last 5 percent of the total life. Thus, separation is a fair measure of crack initiation life and is used as a definition of crack initiation in this report. In this context, the fatigue life data to be discussed in the ensuing paragraphs are useful only in predicting the formation of cracks on the order of 0.1 inch long or smaller. It is noteworthy that such an initial crack length is convenient for use in fracture predictions of flaw growth which typically utilize initial flaw sizes on the order of 0.010 to 0.10 inch (e.g., Reference 6).

The influence of last of the above-noted factors – the presence of inhomogeneities and flaws – is often manifest in a reduction in the number of cycles spent in crack initiation. Additionally, depending on the relative size and character of inclusions, their presence may likewise reduce the crack-propagation period. This factor, however, does not adversely effect the usefulness of the data reported because similar inclusions and flaws exist in the actual rail. But care must be exercised to ensure that differences in the probabilistic distributions of the sizes and locations of inclusions and flaws between test specimens and rails are accounted for (perhaps by the use of available models). With these considerations in mind, the fatigue life characteristics of uniaxial small-diameter rail steel samples will now be examined.

Fatigue resistance of the rail steel is reported in this section for a variety of strain controlled conditions. Included are results obtained from extensive testing under constant amplitude fully reversed and nonfully reversed (mean stress) conditions. Also reported are results from systematic testing that interspersed initial cyclic compression prestrain and periodic overstrain histories in otherwise constant amplitude fully reversed histories. A total of 36 samples of HR and CR material have been committed to this study. Data obtained from the fully reversed baseline condition have been reduced and plotted in Figure 10 on coordinates of strain and life in the manner detailed in Reference 3. Results developed using the nonfully reversed control condition are presented in Figure 11 on coordinates of the product of stable maximum stress and the strain amplitude and life. The use of this product as a basis for consolidating mean stress effects in fatigue has been suggested by Smith, et al[7]. It has recently been derived as a special case of a more general energy-based damage parameter.[8]

Since too few data are available for the nonconstant amplitude histories to warrant graphical presentation, results of these tests will be reported later when compared with the baseline data.

The constant amplitude fully reversed data shown in Figure 10 represent results of tests performed on HR longitudinal samples of the rail steel. Examination of the fracture surfaces of these specimens indicated the initiation/propagation process began at the free surface, the crack propagating in an intragranular manner and terminating in unstable cleavage mode without shear-lip formation as typified by the macrograph shown in part (a) of Figure 12.

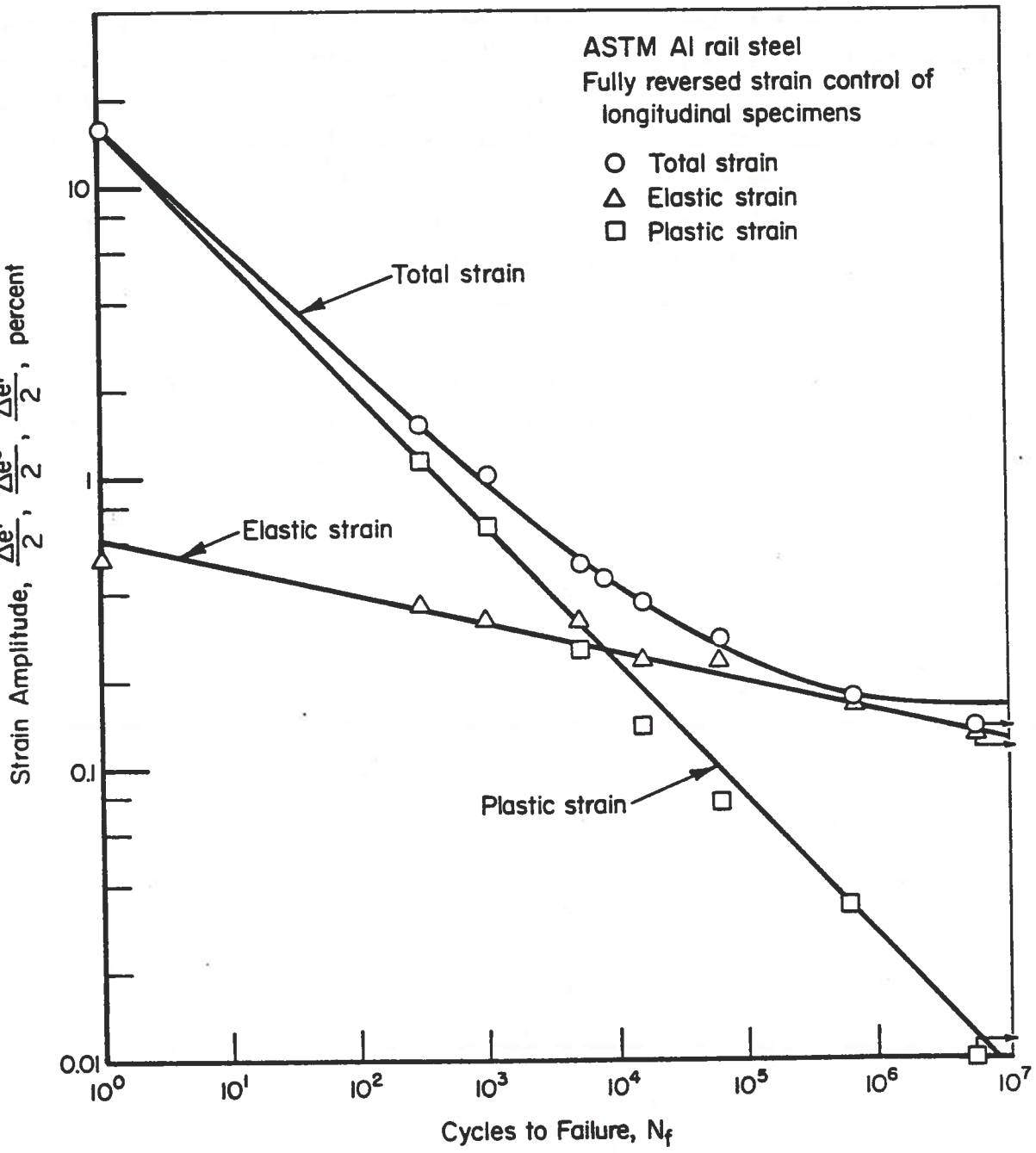

FIGURE 10. FATIGUE RESISTANCE OF THE RAIL STEEL AS A FUNCTION OF APPLIED STRAIN

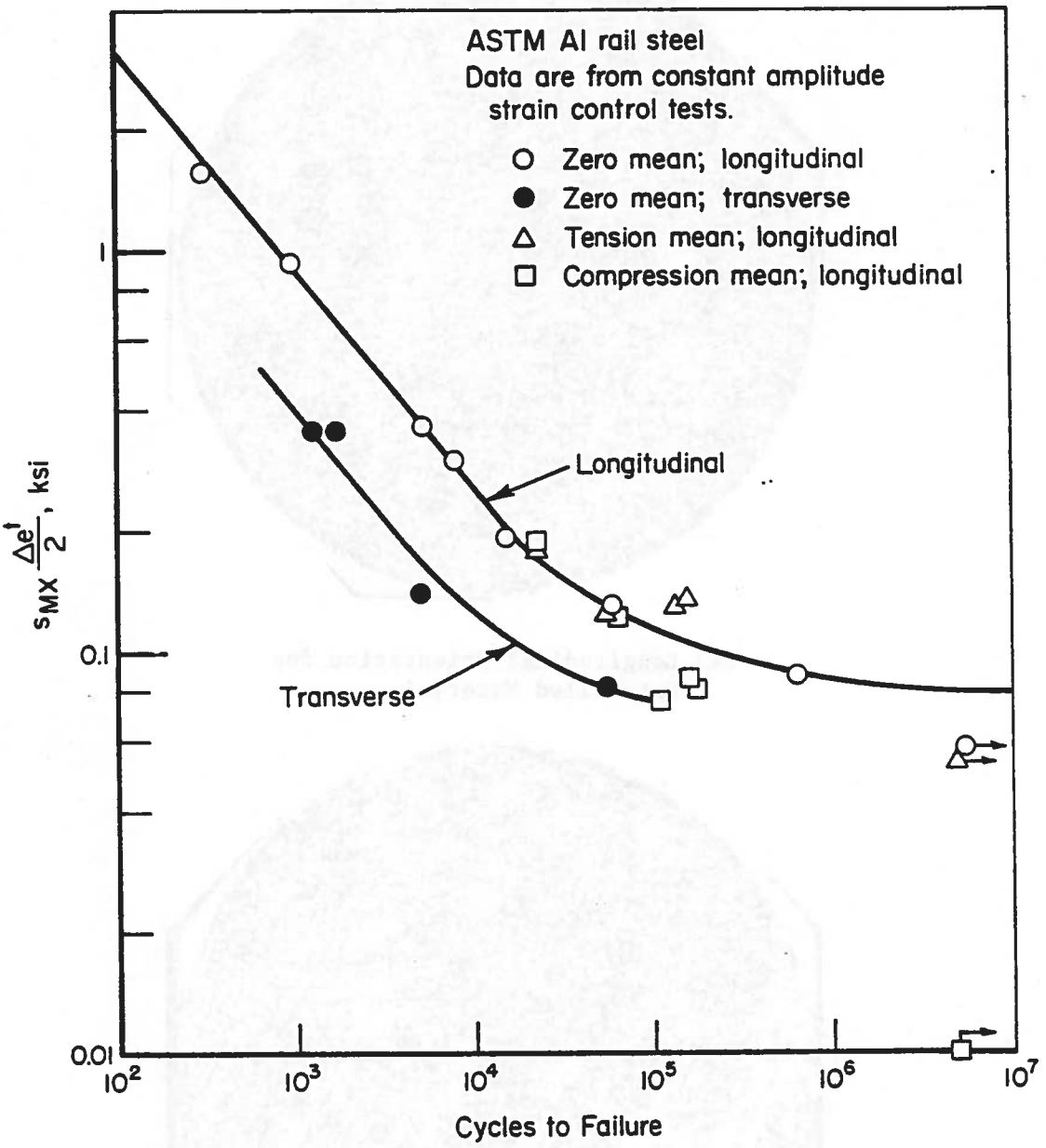

FIGURE 11. FATIGUE RESISTANCE OF THE RAIL STEEL AS A FUNCTION OF THE PARAMETER $s_{MX}\Delta e^t/2$

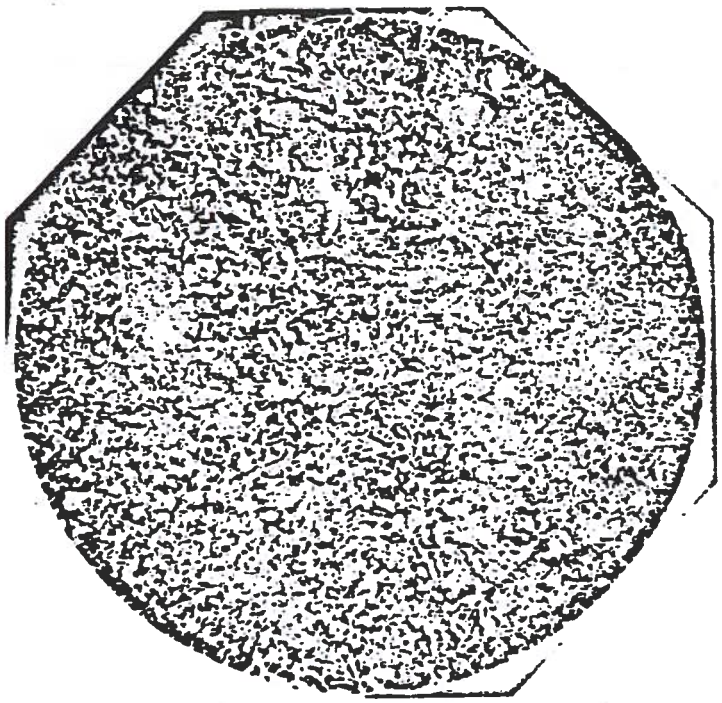

(a) Longitudinal Orientation for
Hot-Rolled Material

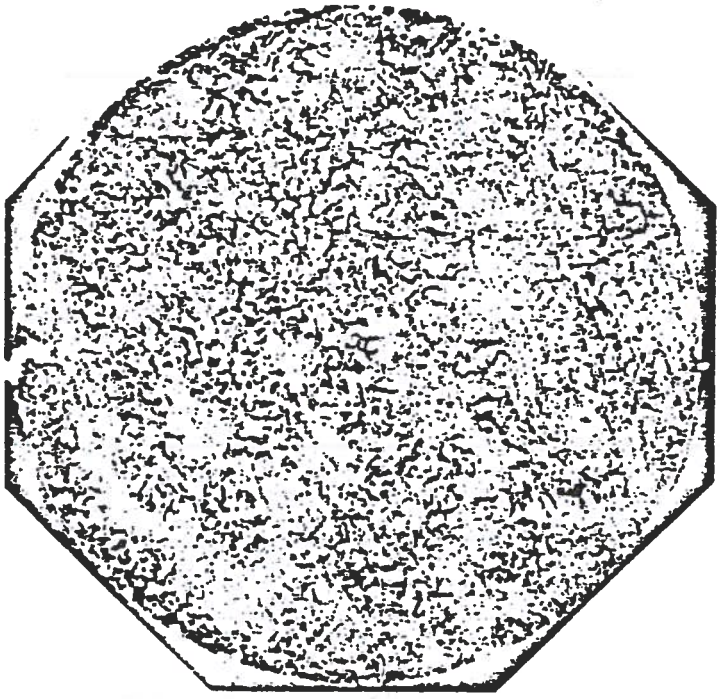

(b) Transverse Orientation for
Hot-Rolled Material

FIGURE 12. TYPICAL FRACTURE SURFACES

In many cases, the fracture surface showed evidence of multiple initiation (as many as three sites in some instances). However, in no case were these initiation sites observed to be related to metallurgical inhomogeneities or flaws discernible at a magnification factor of 10. Furthermore, no "inside-out" failures (typically encountered in dealing with metals whose fatigue resistance is controlled by void/inclusion initiation sites) were noted in this cursory metallographic study. These two facts suggest that the data of Figure 10 should be tempered by the results of probabilistic flaw/inclusion distribution models before being used in predictive models of the fatigue resistance of actual rail.

Comparison of the data shown in Figure 10 with that in the literature for intermediate carbon and alloy steels measured in terms of fatigue strength-based parameters as reported in Table 2 shows the fatigue resistance of this steel to lie slightly below the trend for steels of comparable hardness[9]. However, its resistance as assessed in terms of fatigue ductility-based parameters listed in Table 2 lies above the corresponding trend[9]. In contrast to observed differences in these measures of fatigue resistance between this rail steel and trends established for other steels, the transition fatigue life corresponds closely with the trend value for steels of comparable hardness. As expected, in view of the above-noted trend in stress-based resistance, the fatigue limit for the steel lies below that observed for steels of comparable hardness by about 18 percent. Finally, it should be noted that the total strain-life behavior shown in Figure 10 can be analytically characterized using the empirical strain life equation suggested by Morrow[3], the constants as well as the equation being reported in Table 2.

Consider now the effects of mean stress and transverse specimen orientation on the fatigue resistance of the rail steel. In order to establish the extent to which these effects alter the fatigue resistance as compared to that for longitudinal samples tested under fully reversed control conditions, use must be made of a fatigue damage parameter which provides an equivalence condition between differing control conditions for equal fatigue damage. This report utilizes the previously introduced parameter $s_{mx}\Delta e^t/2$[7] for this purpose. This parameter has been shown to achieve high consolidation for a variety of steels and other metals[7,10]. Fatigue life data in Figure 10 have been replotted in terms of the damage parameter $s_{mx}\Delta e^t/2$ in Figure 11 (open circular symbols). Also shown on this figure are data from tests of transverse samples (solid circles) and from tensile and compressive mean stress tests (open triangles and open squares, respectively.

It is clear from the data shown in Figure 11 that HR transverse samples have significantly less fatigue resistance as compared to the corresponding longitudinal data. Some insight as to the cause of this reduced resistance is gained from a macroscopic examination of the fracture surface. It is apparent from such studies that the fracture surfaces of all transverse samples included an apparent delamination flaw region as shown in Figure 12(b). Such a flaw lying in a plane perpendicular to the loading axis would be expected to initiate fatigue cracks almost immediately after strain cycling commences. Assuming that such initiation occurred with the first cycle, the total life of the transverse specimens would be spent in propagation — a seemingly realistic circumstance as evident in the close correspondence between propagation periods in longitudinal samples and the total life of transverse samples, especially at the lower strain level. Given that such a circumstance prevails, predictive models for the initiation and growth of longitudinal vertical and horizontal flaws would best be based on fracture mechanics principles.

Consider now the role of mean stress in altering the HR rail steels fatigue resistance as compared to fully reversed conditions. Fatigue-life data for a range of mean strains and strain amplitudes are shown in Figure 11 along with the corresponding zero mean strain case. Mean stress data are available for only a small range of lives because, as noted earlier, at higher strains (and shorter lives) mean stress relaxes quickly to the fully reversed state while at smaller strains negligible fatigue damage is accumulated so that failure does not occur. It is apparent from Figure 11 that values of $s_{mx}\Delta e^t/2$ from about 0.20 to 0.07 ksi bracket these limiting conditions. Between these values, the parameter achieves a very high data consolidation at shorter lives ($N_f < 100{,}000$ cycles) of both the tensile and compressive mean stress data. But at longer lives the scatter is somewhat greater, a factor in life of about 2.5 for tensile mean stress data and 10 for compressive mean stress data. Note that fracture surfaces of all mean stress test samples are similar to that for the fully reversed case (e.g., as shown in Figures 12(a) and 12(b).

Let us next examine the role of initial compressive cyclic prestrain, periodic overstrain interspersed with constant amplitude cycles, and initial cold working, in altering the fatigue resistance as compared to the constant amplitude resistance of the HR material.

The initial compression cyclic prestrain history consisted of 50 cycles of zero-compression cycling at a strain range of 0.50 percent. Such

compression precycling is said to cause crack initiation fatigue damage in the form of surface roughing which serves to reduce the total life substantially more than indicated by linear cumulative damage theory. After the application of the cyclic prestrain, linear damage theory would indicate about 99 percent of the life remains. For the cases examined (0.165, 0.18, and 0.36 percent strain amplitude after initial compression cycling), the results obtained for the intermediate amplitude shows that significantly more damage occurred than indicated by linear damage since only 69 percent of the life remained on a strain-life assessment basis. The stable compressive mean stress present over the life in this case tends to reduce the apparent impact of the prestrain. If the influence of mean stress is considered in terms of the mean stress damage parameter, the compressive cyclic prestrain reduces the life by a factor of about 10 as compared to the baseline case. (Note that no failure occurred at the lower level.) At the largest strain amplitude, the deformation response was essentially fully reversed and compared closely to that of the baseline case. The life was slightly longer (5 percent), an observation attributed to the small stable compression mean stress. The action of the prestrain in reducing the life is not evident at this larger amplitude. This is, however, to be expected in view of the large plastic strain component active throughout the entire fatigue life. These results indicate that large compression cycles early in the life of a rail steel can significantly reduce its fatigue resistance at lower strain amplitudes, approaching the endurance strain level. In the context of predictive models for rail fatigue resistance, they suggest that events in the service loading which cause compression overstrains early in life do more extensive damage than would be expected based on linear damage theory. Such a history dependence of the damage rate can be conservatively accounted for by using initial compression precycled life data as a basis for damage assessment in predictive models.

Consider now the influence of periodic overstrains in reducing the fatigue resistance as compared to baseline constant amplitude data. Three basic types of history have been examined – those which induce either tension or compression mean stress and that which induces zero mean stress. (Unfortunately, extensometer drift during the last test case invalidates the result and precludes its inclusion and discussion herein.) In all test cases, the history consisted of a 100 percent overstrain interspersed in constant amplitude cycles of 0.18 percent amplitude every 10^5 cycles in one tensile mean stress case and every 2.5×10^4 cycles in each of the tensile and compressive mean stress cases. The stress response in both tensile cases was similar, the

mean remaining in, even at 10^5 cycle intervals. Thus, as might be expected, the lives were similar; 50 percent of the baseline life for the larger interval and 59 percent for the shorter. Results for the compression case using the same prestrain range and history showed the life to be 107 percent greater than the baseline fully reversed case. Damage due to the periodic overstrain assessed on a linear strain-life basis for the 10^5 cycle interval is 1.8×10^{-4} while that for the 2.5×10^4 cycle interval is 9.1×10^{-4} for the tension mean case and 3.2×10^{-3} for the compression case. In all cases this increment of damage is very small — it, therefore, cannot account for the observed differences in relative fatigue resistance on a strain life basis. Clearly the mean stress, albeit small, is again a dominant factor. Yet when examined in the context of the mean stress parameter, the action of the mean stress also fails to account for the absolute difference in fatigue resistance between these periodic overstrain data and that for constant amplitude cycling, as evident in Figure 13. It is apparent from this figure than whenever some sequence of nonconstant amplitude cycles is interspersed in an otherwise constant amplitude history, the fatigue resistance at longer lives is reduced substantially. Such an effect has been previously observed in many metals[11]. In some steels, this sequence effect wipes out the fatigue (endurance) limit; such is, however, not observed in the rail steel examined herein. In the context of predictive models of rail fatigue resistance, these sequence effects can be simply accounted for by using such data to calibrate the damage-life relationship.

Finally consider the influence of cold work on the fatigue resistance of the HR rail material. Results of two constant amplitude tests show the long life fatigue resistance of the CR material to be superior to that of the baseline material when assessed in terms of the damage parameter, $s_{mx}\Delta e^t/2$. This is to be expected in view of the changes in hardness caused by rolling which suggests that the fatigue resistance at 5×10^5 cycles increases substantially, as evident in Figure 14. However, when the fatigue resistances are compared on the basis of total strain, the results show the HR material to be marginally superior. This apparent discrepancy can be explained in view of the larger stresses that correspond to a given strain amplitude for the CR material as compared to the HR material. Even though at shorter lives a strain based assessment shows the HR material to be superior, the projected long life fatigue resistance (assuming the elastic strain life behavior dominates this situation) for the CR material shows that the increased resistance expected in view of hardness changes will be achieved. (This projection was

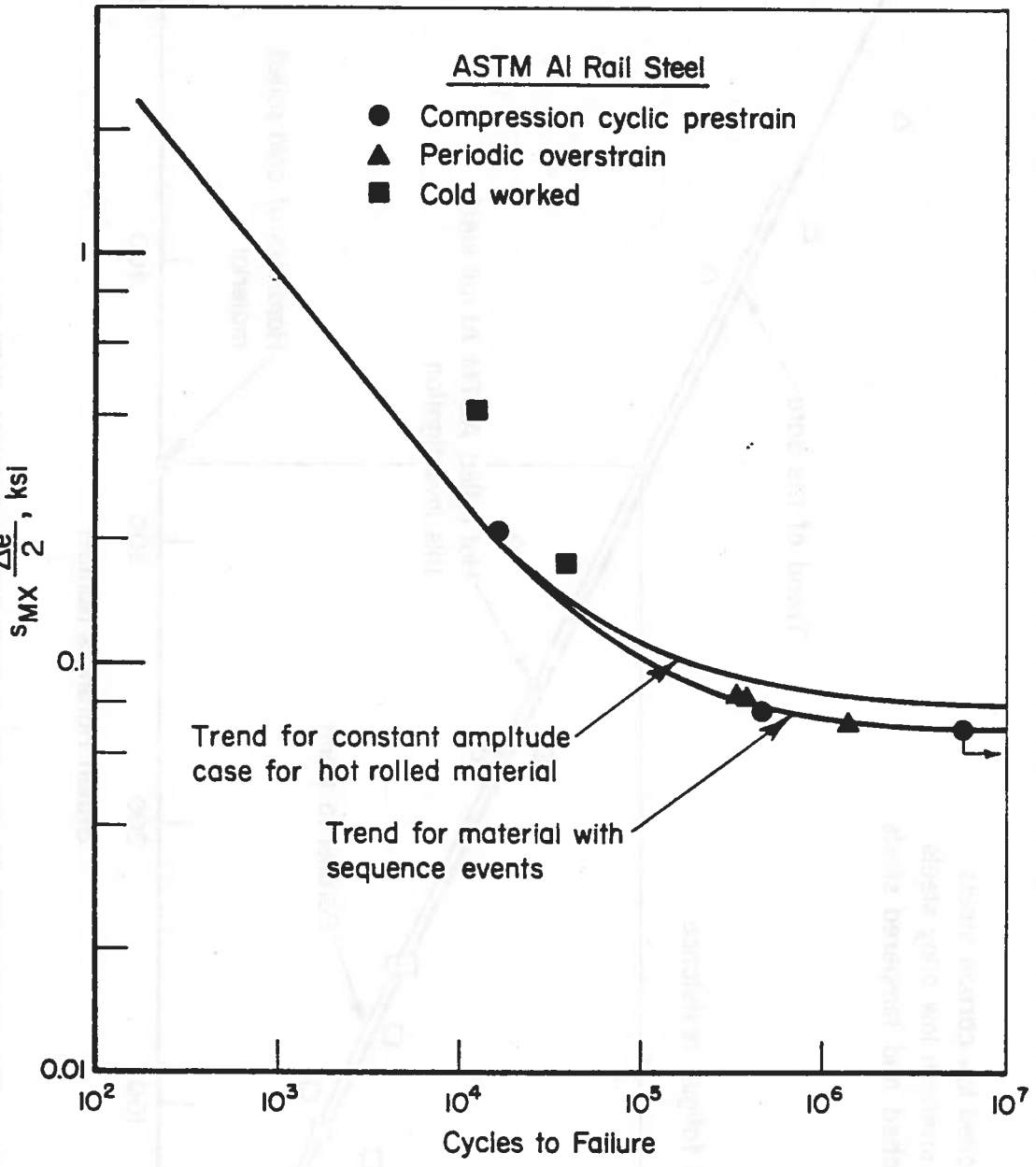

FIGURE 13. HISTORY EFFECTS ON THE FATIGUE RESISTANCE OF THE HR MATERIAL

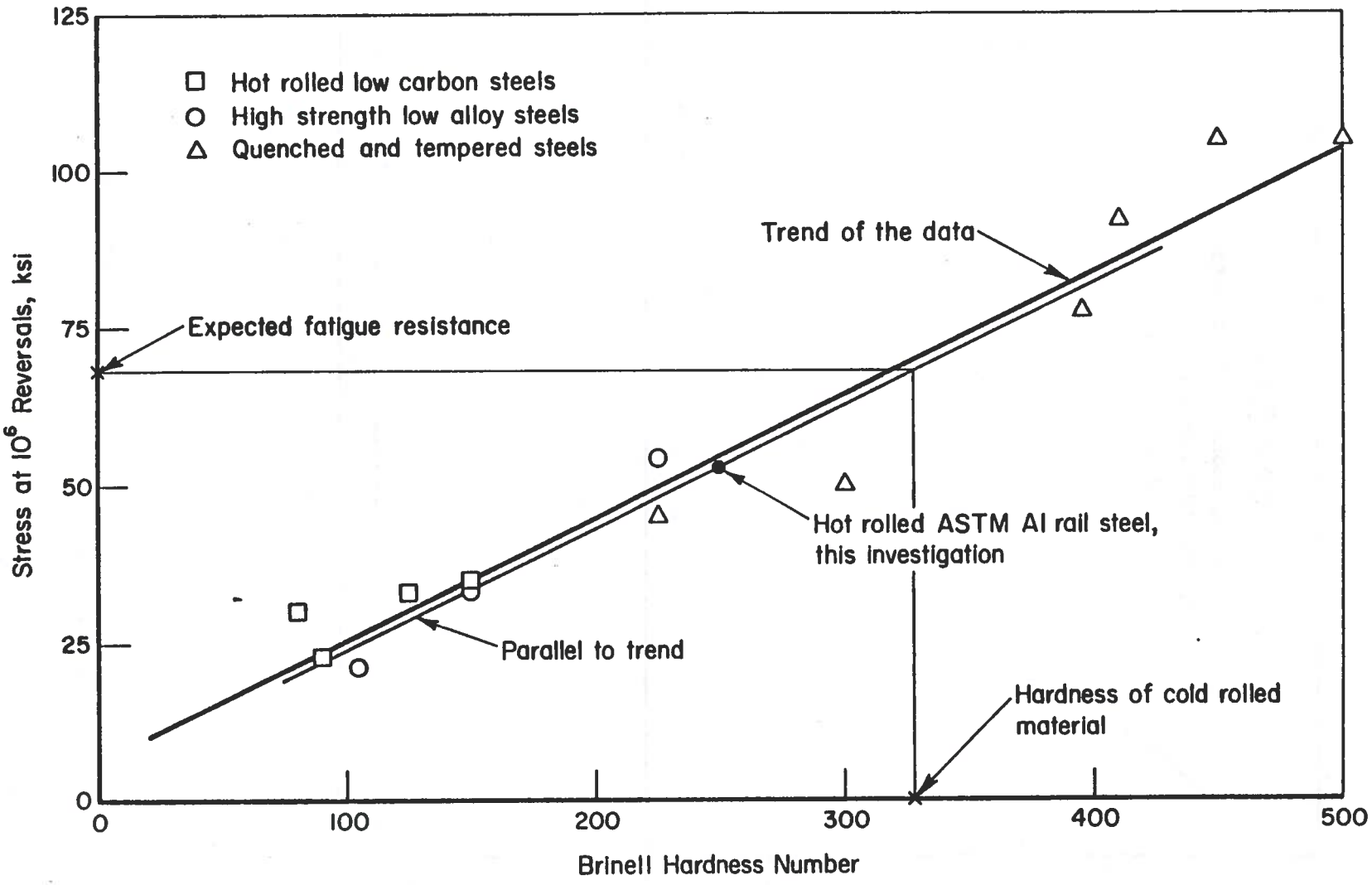

FIGURE 14. THE DEPENDENCE OF FATIGUE RESISTANCE ON BRINELL HARDNESS NUMBER

established using the fatigue strength coefficient of the HR material as one point and the elastic strain and life from a test of the CR material as the second point to establish the Basquin relationship.) The fatigue resistance at 5×10^5 cycles so projected was 0.231 percent strain amplitude while that based on hardness was 0.24 percent strain amplitude. Like the results which showed the HR material to be sensitive to sequence, this dependence of the material fatigue resistance on relative hardness should be incorporated in any rail flaw initiation-prediction model. The damage life relationship could be periodically (or continuously) updated as a function of hardness which in turn, could be prescribed as a function of some variable like cumulative plastic strain that is computed in such models.

MATHEMATICAL MODELS OF MATERIAL CYCLIC INELASTIC DEFORMATION RESPONSE

Throughout the report, the static and cyclic deformation response and fatigue resistance of a rail steel determined using small diameter uniaxial test specimens have been reported and discussed in the context of predictive models for rail failure. One of the more vexing problems encountered in using these data in such predictive models resides in the use of uniaxial stress data developed under constant amplitude control conditions in situations where the stress state is multiaxial and the service loading significantly different from that used to develop the data.

The extension of data developed under uniaxial constant amplitude conditions to deal with multiaxial variable amplitude loading requires (1) an equivalence condition between stress states for both deformation and fatigue and (2) a means of resolving variable amplitude cycles into equivalent constant amplitude cycles which cause equal fatigue damage. This section focuses on one related aspect – constitutive equations for the cyclic inelastic deformation response of time and rate independent metallics subjected to variable amplitude mechanical cycling under isothermal conditions. Consideration is given only to cases where the strains and their gradients are small. First, the general theory is discussed. Thereafter, situations in which both the loading and the stressing are proportional are studied and models are developed for the rail steel discussed in this report.

General Constitutive Formulation

It is clearly evident from a variety of experimental studies that, under nonviscous flow, the yield surface may change its shape as well as either translate or expand during the course of plastic straining[12]. Considering an initially isotropic material, this yield surface has the general form (for small strains and strain gradients):

$$f = f(\underset{\sim}{s}, \underset{\sim}{\alpha}, \lambda) = 0 \quad ; \tag{1}$$

including one tensor and one scalar hardening parameter. Here f is an isotropic function of the deviatoric stress tensor, $\underset{\sim}{s}$. When $\underset{\sim}{\alpha} = 0$, Equation (1) has the form:

$$f = f(\underset{\sim}{s}) - F(\lambda) = 0 \quad ; \tag{2}$$

the yield surface shape remains constant, uniformly expanding (or shrinking) in accordance with the scalar parameter λ. Useful measures of the parameter λ are current values of the invariant of plastic strain rate, $\dot{e}^{p}_{ij}$ (necessarily deviatoric assuming incompressability), and the dissipation function, $s_{ij}\,\dot{e}^{p}_{ij}$. (The symbol ($\dot{}$) denotes a time rate of change.) Equation (1) can also be rewritten:

$$f = f(\underset{\sim}{s} - \underset{\sim}{\alpha}) - C = 0 \quad . \tag{3}$$

For this particular case where $F(\lambda)$ = constant, the initial yield surface undergoes rigid-body translation with varying $\underset{\sim}{\alpha}$ representing the center of the surface.

It is clear from the above that Equation (1) embodies the special hardening rules known respectively as "isotropic", Equation (2) and "kinematic", Equation (3). It is well known that neither of these rules can characterize the change in shape of the yield surface observed in experimental studies of nonproportional plasticity and prestrain effects. To be sufficiently general, Equation (1) must be rewritten to embody both translation and expansion, or $\underset{\sim}{\alpha}$ must be made to depend on the entire deformation history. By requiring that f be an even homogeneous function of $\underset{\sim}{s} - \underset{\sim}{\alpha}$, in addition to being an isotropic function of $\underset{\sim}{s}$ and $\underset{\sim}{e}^{p}$, Equation (1) is capable of simulating nested surfaces as well as translation with varying $\underset{\sim}{\alpha}$ representing the center of the surfaces(s). It remains to specify the dependence of $\underset{\sim}{\alpha}$ and λ on the strain history.

During any plastic strain increment, there is a variation in both hardening parameters. For the tensor parameter specifying translation, there are several basic rules: that of Prager and others[13]

$$\dot{\underset{\sim}{\alpha}} = a\,\dot{\underset{\sim}{e}}^{p} \tag{5}$$

and its modification by Shield and Ziegler[14]

$$\dot{\underset{\sim}{\alpha}} = b(\underset{\sim}{\sigma} - \underset{\sim}{\alpha})\,\dot{\underset{\sim}{e}}^{p} \tag{6}$$

and that of Eisenberg and Phillips[15]

$$\dot{\underset{\sim}{\alpha}} = c(\lambda)\,\dot{\underset{\sim}{e}}^{p} + \frac{dc}{d\lambda}\,\underset{\sim}{e}^{p}\,\dot{\lambda} \quad . \tag{7}$$

Others incorporate the form of Equation (6) in terms of joint invariants of deviatoric stresses and strains. The scalar parameter specifying the expansion of the surface can be chosen as it has been for the case of isotropic

hardening discussed earlier. Note that by the inclusion of a second tensor valued function of at least the plastic strain to impact on the shape of the yield surface, the dependence of $\underset{\sim}{\alpha}$ on the history is simplified. One is, however, left with at least as complicated a description of the yield surface[16].

Following the classical formulation, the associated flow rule has the form

$$\dot{\underset{\sim}{e}}^{p} = \frac{\partial f}{\partial \underset{\sim}{s}} \dot{\kappa} \quad , \tag{8}$$

satisfying the normality condition of the plastic strain increment, $\dot{\underset{\sim}{e}}^{p}$, to the corresponding yield surface at the stress point. In equation (8), κ is a positive scalar chosen such that the stress point remains on the surface during plastic flow (the consistency condition); that is,

$$df = \frac{\partial f}{\partial \underset{\sim}{s}} (\dot{\underset{\sim}{s}} - \dot{\underset{\sim}{\alpha}}) = 0 \quad , \tag{9}$$

where $F(\lambda)$ is assumed constant.

Complete characterization of the deformation response of a generic element of material requires that the above flow rule be coupled with a description of the elastic response of the material. Again following the classical formulation, it is assumed that the total nonviscous strain component can be decomposed into an elastic and plastic part. Thus

$$\dot{\underset{\sim}{e}}^{t} = \dot{\underset{\sim}{e}}^{e} + \dot{\underset{\sim}{e}}^{p} \tag{10}$$

Appropriate measures of the elastic strain components are detailed elsewhere[17]. A number of specific formulations have been advanced for this general class of cyclic deformation response (e.g., see Reference 18). Their discussion is, however, beyond the scope of the present section.

Models of Proportional Cyclic Plasticity

Generalized Stress/Strain Space for Stable Materials

In the context of the formulation presented in the previous section, that of the present section is greatly simplified in that the dependence of $\underset{\sim}{\alpha}$ on the invariants (or joint invariants) of stress and strain can be simply prescribed for a given material. It is no longer a continuously varying

tensor function of the entire history. The situation is further simplified since stresses and strains in the generalized three-dimensional space can be related to that of a uniaxial test through the use equivalence[17] quantities based on the second invariant of the deviatoric stress and strain tensors (isotropy implied). Through their introduction the entire character of the yield surface can be described by a single parameter. Specifically, the theory[19] characterizes material deformation response in terms of hysteresis loop shape and the Masing[20] (kinematic) hardening rule applied in accordance with the materials memory of prior deformation.

In general, the constitutive equation has the form

$$G(\underset{\sim}{s}, \underset{\sim}{e}) = 0 \quad , \tag{11}$$

where G is a functional with domain over time, t. It is assumed that the principal stresses are proportional and constant in direction. Furthermore, it is assumed that only the most recent sign reversal of stress and strain governs the loop shape. This means that stress $\underset{\sim}{s}$ is a function of strain $\underset{\sim}{e}$, as well as the stress $\underset{\sim}{s}_i$, and strain $\underset{\sim}{e}_i$, at the most recent reversal, (here i denotes the most recent reversal). In general, this relationship exists in six dimensional stress and strain space. Equation (11) becomes

$$\underset{\sim}{s} = \underset{\sim}{f}_i \, (\underset{\sim}{e}) \quad , \tag{12}$$

where $\underset{\sim}{f}_i$ is an odd vector function valid for the stress-strain path between t-strain rate reversals i and i + 1. The totality of all such paths may be written

$$\underset{\sim}{s} = \underset{\sim}{f}_i(\underset{\sim}{e}, \underset{\sim}{e}_i, \underset{\sim}{s}_i) \tag{13}$$

specifying stress as a function of strain when the point $P_i = (s_i, e_i)$ is given. It is assumed that the hysteresis loops close for the material; that is, the material is cyclically stable. Thus,

$$\underset{\sim}{s}_{i+2} = \underset{\sim}{f}_{i+1}(\underset{\sim}{e}_{i+2}, \underset{\sim}{e}_i, \underset{\sim}{s}_i) \tag{14}$$

holds for all points P of strain rate reversal. Then, if for the displacements, $\underset{\sim}{u}_{i+2} = \underset{\sim}{u}_i$ and for the tractions $\underset{\sim}{T}_{i+2} = \underset{\sim}{T}_i$, it is clear that the equations of motion and constitutive equation are satisfied at t_{i+2} if they are satisfied at t_i. The argument may be extended to any point pair $t = t_i + \tau$ and $t = t_{i+2} + \tau$ to show that the hysteresis loops in load space coincide under cyclic loading

at all intermediate points as they do at the points of strain rate reversal. Now let the ascending (i even) and descending (i odd) branches of all material hysteresis loops be congruent and further contruent with the first ascending branch from the unstressed state (i = 0). Then the monotonic curve and the cyclic stress-strain curve are identical (because the material is cyclically stable) and are given by a "Masing transformation" of Equation 13. By this is meant that these two curves are congruent with the hysteresis loop branches scaled in both stress and strain by a factor of ½. Let the loops be described by the function f (which is necessarily odd):

$$\underset{\sim}{\sigma} - \underset{\sim}{\sigma}_i = \underset{\sim}{f}_i(\underset{\sim}{\varepsilon} - \underset{\sim}{\varepsilon}_i) \tag{15}$$

Then a Masing relationship exists if the cyclic stress-strain relation is

$$\underset{\sim}{\sigma} = \tfrac{1}{2}\underset{\sim}{f}(2\underset{\sim}{\varepsilon}) \tag{16}$$

It is seen[19] that the Masing relationship holds in cyclic force-deformation space when deformations are small (i.e., the equation of motion is linear in all arguments).

As presented, the theory is valid for generalized states of stress and strain, the multiaxial nature being embodied in equivalence quantities which are unique functions of their tensor valued counterparts under the action of proportional stressing. These quantities must, however, be defined in terms of ranges to have nonzero values. There are, of course, other formulations for this class of loading[21]. They are beyond the scope of the present report whose purpose it is to provide background to the model of rail steel deformation based on the previously discussed experimental data.

Uniaxial Cyclic Loading for Nonstable Materials

Building from the basic assumptions of the preceding theory in the context of Morrows'[3] observations of material cyclic deformation response, we couple a model for loop shape with the Masing kinematic hypothesis applied in accordance with the materials memory for prior deformation. Loop shape is modeled by a Masing transformation of the cyclic stress strain curve analytically depicted as

$$\frac{\Delta e^t}{2} = \frac{\Delta s}{2E} + \left(\frac{\Delta s}{2K}\right)^{1/n} . \tag{17}$$

The symbols n and K are best fit to model the appropriate stress-strain curve, as detailed previously for the rail steel in Table 2 for both monotonic and stable cyclic response. Memory can be achieved in a number of ways, depending largely on how Equation (17) is represented for computational purposes. Such detail is, however, beyond the scope of the present report.

The transient response between monotonic and stable cyclic conditions can be modeled simply in terms of adjustments to the intercept (stiffness) K and the exponent (hardening rate) n in Equation (17) as a function of some parameter which is a simple, continuous measure of the transient; say cumulative plastic strain amplitude. Following this premise and rewriting Equation (17) to accommodate the coupled hardening-softening response of the material, one obtains for the HR rail steel material

$$\frac{\Delta e^t}{2} = \frac{\Delta s}{57.5 \times 10^3} + 0.004 \left(\frac{\Delta s}{130}\right)^{1/n} \tag{18}$$

where n is a function of cumulative plastic strain amplitude given by

$$n = 0.25 \left(\sum_i \frac{\Delta e_i^p}{2}\right)^{0.0495} . \tag{19}$$

Mean stress relaxation can likewise be modeled by appropriate changes in the stiffness coefficient of Equation (17). Based on the observed response of the HR rail steel material, the stress on the nth cycle, s_n, is related to the initial stress, s_i, by

$$s_n = s_i N^r \tag{20}$$

where N is the number of cycles and r is given by $r = 8.8(\Delta e^p)^{1.47}$.

More sophistocated models could of course be developed for modeling both transient and stable response. The extent to which these refinements would improve actual predictions depends largely on the adequacy of those presented to accurately portray actual behavior. Comparisons of actual and predicted response using the present models indicates that further refinements are unwarranted. While further refinements of the uniaxial model may not be warrented to model uniaxial response, there is a need to expand these models to deal with multiaxial states of stress for both proportional and nonproportional loading. At present stable cyclic response can be simulated for these more general problems. Transients which significantly alter uniaxial stress

response are, however, as yet not included in these models. The fact that this analytical capability remains undeveloped is due possibly to the attendant mathematical complexity and to the fact that much needed experimental data remains undeveloped. Before adequate models of rail failure can be evolved, such analytical models and materials data will have to be developed.

SUMMARY AND CONCLUSIONS

This report has examined the monotonic and cyclic deformation response and fatigue life characteristics of a rail steel. Results were presented in light of predictive models for rail fatigue resistance with particular attention being paid to the influence of stress multiaxiality.

Conclusions which can be drawn from the experimental aspects of the deformation and fatigue character of a rail steel follow:

- The ASTM A1 rail steel undergoes significant cyclic softening at lower inelastic strains while at larger strain levels the metal cyclically hardens;
- Stable deformation response for this rail steel is similarly characterized by either single specimen or incremental step test data;
- Relaxation rates for this rail steel are similar under comparable control conditions for each of tensile and compressive mean stresses;
- Relaxation rates under differing combinations of the control mean strain and cyclic range can be rationalized on the basis of the plastic strain range;
- The fatigue resistance of longitudinal samples of this rail steel falls slightly below that for a variety of intermediate carbon steels and alloy steels;
- The fatigue resistance of transverse samples falls significantly below that for longitudinal samples, and finally;

- Compression precycling and period overstrains significantly reduce the life of the rail steel as compared to that anticipated on the basis of a linear damage theory, without consideration for sequence effects.

REFERENCES

1. Johns, T. G., and Davies, K. B., "Preliminary Description of Stresses in a Railroad Rail", Report Number FRA-ORD-71-35, Battelle's Columbus Laboratories, November 1976.

2. Feltner, C. E., and Mitchell, M. R., "Basic Research on the Cyclic Deformation and Fracture Behavior of Materials", in Manual on Low-Cycle Fatigue Testing, ASTM STP 465, 1969, pp 100-128.

3. Morrow, J., "Cyclic Plastic Strain Energy and Fatigue of Metals", in Internal Friction, Damping, and Cyclic Plasticity, ASTM STP 378, 1965, pp 45-84.

4. Dugdale, D. S., "Stress-Strain Cycles of Large Amplitude", J. Mechanics and Physics of Solids, Vol. 7, 1959, pp 135-142.

5. Marich, S., Association of American Railroads, Private communication, April 1977.

6. Anon., "Airplane Damage Tolerance Design Requirements", Military Specification, USAF, MIL-A-83444 (tentative), May 1974.

7. Smith, K. N., Watson, P., and Topper, T. H., "A Stress-Strain Function for the Fatigue of Metals", J. of Matls., JMLSA, Vol. 5, (4), December 1970, pp 767-778.

8. Leis, B. N., "An Energy-Based Fatigue and Creep-Fatigue Damage Parameter", Trans. ASME, J. of Pressure Vessels and Piping, Vol. 99, November 1977, ASME Paper No. 77-PVP-3.

9. Landgraf, R. W., "The Resistance of Metals to Cyclic Deformation", in Achievement of High Fatigue Resistance in Metals and Alloys, ASTM STP 467, 1970, pp 3-36.

10. Jaske, C. E., Feddersen, C. E., Davies, K. B., and Rice, R. C., "Analyses of Fatigue, Fatigue Crack Propagation, and Fracture Data", NASA CR-132332, November 1973.

11. Brose, W. R., Dowling, N. E., and Morrow, J., "Effect of Periodic Large Strain Cycles on the Fatigue Behavior of Steels", SAE Paper No. 740221, 1974.

12. Szczepinski, W., and Miastkowski, J., "An Experimental Study of the Effect of Prestraining History on the Yield Surfaces of an Aluminum Alloy", J. Mechanics and Physics of Solids, Vol. 16, 1968, pp 153-162.

13. Prager, W., "A New Method of Analyzing Stress and Strain in Work Hardening Plastic Solids", J. Applied Mechanics, Vol. 23, 1956, pp 493.

14. Ziegler, H., "A Modification of Prager's Hardening Rule", Q. Applied Mathematics, Vol. 17, 1959, pp 55-60.

15. Eisenberg, M. A., and Phillips, A., "On Nonlinear Kinematic Hardening", Acta Mech., Vol. 1, 1965, pp 81-92.

16. Shiratori, E., and Ikegami, K., "Studies of the Anisotropic Yield Condition", J. Mechanics and Physics of Solids, Vol. 17, 1969, pp 474-491.

17. Hill, R., Mathematical Theory of Plasticity, Clarendon Press, 1950.

18. Mroz, Z., Mathematical Models of Inelastic Material Response, University of Waterloo Press, 1973.

19. Williams, D. P., Lind, N. C., Conle, F. A., Topper, T. H., and Leis, B. N., "Structural Cyclic Deformation Response Modeling", in Mechanics in Engineering, University of Waterloo Press, 1977.

20. Masing, G., "Wis Veröff aus. Siemens Konzern", III Band, 1927.

21. Leis, B. N., Meister, R. P., and Williams, R. S., "Cumulative Damage Analysis and Nondestructive Inspection for Application to Tubular Steel Marine Structures", Battelle Contractor Report Number N0906-8801/1, Battelle's Columbus Laboratories, July, 1976.